Atmos. Chem. Phys. Discuss., 11, 3529–3578, 2011
www.atmos-chem-phys-discuss.net/11/3529/2011/
doi:10.5194/acpd-11-3529-2011

Atmospheric Chemistry and Physics Discussions

Field determination of biomass burning emission ratios and factors via open-path FTIR spectroscopy and fire radiative power assessment: headfire, backfire and residual smouldering combustion in African savannahs

M. J. Wooster[1,2], P. H. Freeborn[1], S. Archibald[3], C. Oppenheimer[4,5,6], G. J. Roberts[1,2], T. E. L. Smith[1], N. Govender[7], M. Burton[8], and I. Palumbo[9]

[1]King's College London, Environmental Monitoring and Modelling Research Group, Department of Geography, Strand, London, WC2R 2LS, UK
[2]NERC National Centre for Earth Observation, UK
[3]Natural Resources and the Environment, CSIR, P.O. Box 395, Pretoria 0001, South Africa
[4]Le Studium, Institute for Advanced Studies, Orléans and Tours, France
[5]Institut des Sciences de la Terre d'Orléans, 1a rue de la Férollerie, Orléans 45071, France
[6]Department of Geography, University of Cambridge, Cambridge CB2 3EN, UK

[7] Scientific Services, Kruger National Park, Private Bag X402, Skukuza, 1350, South Africa
[8] Istituto Nazionale di Geofisica e Vulcanologia, Via della Faggiola, 32-56126 Pisa, Italy
[9] DG Joint Research Centre, Global Environment Monitoring Unit, Ispra, Italy

Received: 1 August 2010 – Accepted: 6 January 2011 – Published: 1 February 2011

Correspondence to: M. J. Wooster (martin.wooster@kcl.ac.uk)

Published by Copernicus Publications on behalf of the European Geosciences Union.

Abstract

Biomass burning emissions factors are vital to quantifying trace gases releases from vegetation fires. Here we evaluate emissions factors for a series of savannah fires in Kruger National Park (KNP), South Africa using ground-based open path Fourier transform infrared (FTIR) spectroscopy and an infrared lamp separated by 150–250 m distance. Molecular abundances along the extended open path are retrieved using a spectral forward model coupled to a non-linear least squares fitting approach. We demonstrate derivation of trace gas column amounts for horizontal paths transecting the width of the advected plume, and find, for example, that CO mixing ratio changes of $\sim$0.001 µmol mol^{-1} ($\sim$10 ppbv) can be detected across the relatively long optical paths used here. We focus analysis on five key compounds whose production is preferential during the pyrolysis (CH_2O), flaming (CO_2) and smoldering (CO, CH_4, NH_3) fire phases. We demonstrate that well constrained emissions ratios for these gases to both CO_2 and CO can be derived for the backfire, headfire and residual smouldering combustion stages of these savannah fires, from which stage-specific emission factors can then be calculated. Headfires and backfires in general show similar emission ratios and emission factors, but those of the residual smouldering combustion stage can differ substantially (e.g., ER_{CH_4/CO_2} up to $\sim$7 times higher than for the flaming stages). The timing of each fire stage was identified via airborne optical and thermal IR imagery and ground-observer reports, with the airborne IR imagery also used to derive estimates of fire radiative energy, thus allowing the relative amount of fuel burned in each stage to be calculated and the "fire averaged" emission ratios and emission factors to be determined. The derived "fire averaged" emission ratios are dominated by the headfire contribution, since the vast majority of the fuel is burned in this stage. Our fire averaged emission ratios and factors for CO_2 and CH_4 agree with those from published studies conducted in the same area using airborne plume sampling, and we concur with past suggestions that emission factors for formaldehyde in this environment appear substantially underestimated in widely used databases. We also find the emission

ACPD
11, 3529–3578, 2011

ratios and factors for CO and NH_3 to be somewhat higher than most other estimates, however, we see no evidence to support suggestions of a major overestimation in the emission factor of ammonia. Our data also suggest that the contribution of burning animal (elephant) dung can be a significant factor in the emissions characteristics of certain KNP fires, and indicate some similarities between the time series of fire brightness temperature and modified combustion efficiency (MCE) that supports suggestions that EO-derived fire temperature estimates maybe useful when attempting to remotely classify fire activity into its different phases. We conclude that ground-based, extended open path FTIR spectroscopy is a practical and very effective means for determining emission ratios, emission factors and modified combustion efficiencies at open vegetation fire plumes, allowing these to be probed at temporal and spatial scales difficult to explore using other ground-based approaches. Though we limited our study to five key emissions products, open path FTIR spectroscopy can detect dozens of other species, as has been demonstrated during previous closed-path FTIR airborne deployments in the same study area.

1 Introduction

Alongside the burning of coal, oil and natural gas, the open combustion of biomass in forest and grassland fires is one of the key pathways by which humans directly affect the atmosphere. The gases and particulates released in biomass burning plumes have substantial short- and long-term chemical, radiative and climatic impacts (Bowman et al., 2009) and proper assessment of these effects generally requires spatio-temporally resolved data on the source emissions magnitude and makeup. This information is usually obtained via multiplication of the mass of dry fuel consumed in the fire [M, kg] by an emission factor [EF_x] representing the amount of chemical species (x) released per kg of dry fuel burned (Andreae and Merlet, 2001). In these calculations, the fuel consumption term is most commonly deduced using satellite-derived burned area measures coupled with estimates of the pre-burn fuel load and combustion completeness

ACPD
11, 3529–3578, 2011

(e.g., Korontzi et al., 2004; van der Werf et al., 2006). Satellite-derived Fire Radiative Power (FRP) observations also enable estimation of fuel consumption, being particularly appropriate when fuel loads are very uncertain (e.g., Reid et al., 2009), where combustion rates rather than totals are required (e.g., Roberts et al., 2009), and/or where near real-time information is needed for operational forecast-type applications (e.g., Kaiser et al., 2009; Xu et al., 2010). In all cases, emissions factors are a vital component of the calculation, and since uncertainties in EF_x propagate linearly onto uncertainties in the derived emissions there is a continued requirement for improved EF_x information and for relationships from which estimates of these maybe better constrained (e.g., Korontzi et al., 2003). This need is increasingly heightened as satellite products related to fuel consumption estimation become more mature (e.g. van der Werf et al., 2006; Roy et al., 2008; Freeborn et al., 2009; Giglio et al., 2009).

At present, the emissions factor for use at a particular fire is usually selected from a published database, commonly that of Andreae and Merlet (2001) and subsequent updates. The estimates of EF_x are derived using a variety of means, commonly via smoke emission ratio measures ($ER_{x/y}$, the relative amounts of two smoke species (x) and (y)). As Keene et al. (2006) suggest, emissions ratios (ERs) and emissions factors (EFs) for many species typically show wide variations with the ratio of live to dead fuel, fuel component physical type, and fuel arrangement and moisture, in addition to ambient environmental conditions and fuel elemental content (e.g., nitrogen and sulphur). For some important species, it has been suggested that changes in fuel and environmental conditions may induce variations of 500% or more in emissions factors (e.g., Griffith et al., 1991), but such variability is often not fully expressed in databases which may only report averages and which generally do not differentiate between different combustion styles (e.g., backfires and headfires; Smith and Wooster, 2005). Furthermore, some databases may only include results from small-scale laboratory experiments, whist others focus on airborne "whole plume" sampling. Both approaches offer advantages, but whilst the former may not be fully representative of open vegetation fire conditions, the latter typically cannot be used to sample the individual fire phases

ACPD
11, 3529–3578, 2011

or stages, and there can be problems in using airborne ER measurements to derive emissions factors and to sample the residual smouldering combustion (RSC) stage (Andreae and Merlet, 2001; Christian et al., 2007; Yokelson et al., 2003; Bertschi et al., 2003). These potential limitations suggest further methodological developments in biomass burning emissions measurements maybe warranted, something the current work aims to contribute to. Furthermore, many of the controls on EFs also regulate combustion efficiency (the ratio of CO_2 to total carbon released in the smoke), whose calculation is usually simplified to one based on CO_2 and CO concentration measures alone (the modified combustion efficiency (MCE) of Ward and Radke, 1993). Since emissions ratios of many species are well correlated to MCE (Sinha et al., 2003a), one goal in current biomass burning research is to identify methods for determining the most appropriate MCE, ER and EF measures for use in fires burning under particular environmental conditions and fuel types. Such research will most likely require sampling the fuel, fire, meteorological and emissions characteristics of large numbers of open vegetation fires. Recently Fernández-Gómez et al. (2011) suggested open path Fourier Transform Infra Red (FTIR) spectroscopy as a potential tool for providing emissions measurements at the site of field-scale open vegetation fires, though their proof-of-concept was confined to a small-scale laboratory setup. An objective of the current work is therefore to evaluate whether ground-based, open path FTIR spectroscopy conducted at the site of real open vegetation fires can provide the necessary information on "plume integrated" smoke chemistry that is commonly required in many biomass burning studies, and also to assess if the technique allows for the study of intra-fire as well as inter-fire emissions variability. We demonstrate the practicalities of deploying OP-FTIR in so-called "long-path" mode (Gosz et al., 1988), measuring smoke trace gas abundances over pathlengths of hundreds of meters, and we evaluate the methods ability to provide high temporal resolution ER and EF data for "naturally burning" vegetation fires. Measurements were conducted concurrently with airborne observations of Fire Radiative Power (FRP) release, allowing the relative amount of fuel burned in the headfire, backfire and residual smoldering combustion stages of the

ACPD
11, 3529–3578, 2011

studied fires to be quantified. This allows $ER_{x/y}$ and EF_x to be determined from the FTIR-derived smoke column abundances retrieved separately for each fire stage, and also through their combination to calculate "fire averaged" quantities. The study was conducted in the savannah environment of Southern Africa, whose fires are annually responsible for perhaps around one quarter of global fire fuel consumption (van der Werf et al., 2003; Roberts et al., 2009; Archibald et al., 2010).

2 Background

2.1 Study of laboratory and open fire plumes

Smoke emission ratios, emissions factors and combustion efficiencies can be deduced from trace gas concentrations measured via a number of approaches. Delmas et al. (1995), Goode et al. (2000), Andreae and Merlet (2001) and Koppmann et al. (2005) include detailed reviews, with laboratory combustion chamber measurements being probably the most common. Here fuel consumption and total gas flux can be accurately logged, enabling direct calculation of EF_x for the separate flaming and smouldering phases, and calculation of so-called "fire-averaged" values via a weighted mean approach. However, fire characteristics in laboratory-scale experiments can differ from natural behaviour, potentially resulting in EF biases (Delmas et al., 1995; Fernández-Gómez et al., 2011). Trace gas measurements for open vegetation fires are therefore greatly valued, but can be difficult to acquire due to fires hazardous, highly dynamic and sometimes unpredictable nature. Furthermore, in open fires all combustion phases maybe occurring simultaneously, with emissions released into one or more "integrating" plumes. Airborne campaigns sample such plumes and offer many practical and scientific benefits (e.g., Yokelson et al., 1999, 2003; Sinha et al., 2003a, 2003b), but logistics and costs can hinder deployments. Since the relative amount of fuel consumed in each phase of the fire is generally unknown when relying on aircraft observations, it is also assumed that natural mixing provides the appropriate averaging (Andreae and

ACPD
11, 3529–3578, 2011

Merlet, 2001). Ground sampling of plumes has most commonly involved canister or grab bag collection and subsequent laboratory analysis. Field-deployed spectroscopic methods potentially avoid the problem of within-canister chemical conversion or wall-loss (Goode et al., 2000; Yokelson et al., 2003), and an FTIR system allows a single instrument to provide the IR spectra from which many gases can be simultaneously and continuously monitored at detection limits of ~5–20 parts per billion or better over ~100 m pathlengths (Griffith et al., 1991; R. J. Yokelson et al., personal communication, 1996, 1999). This ability to target multiple gases simultaneously may be critical for discerning intra-fire emissions ratio variability.

2.2 FTIR smoke plume studies

FTIR-based vegetation fire smoke studies have usually deployed so-called closed-path/extractive techniques, or open path methods covering relatively short (<1–10 m) distances (e.g., Goode et al., 2000; Yokelson et al., 1996, 1999; Bertschi et al., 2003; Christian et al., 2007; Castro et al., 2007; Fernández-Gómez et al., 2011). Whilst these studies have been extremely productive, sample representativeness is still a concern, and it can prove hazardous and difficult to sample areas of higher intensity combustion. An alternative strategy is offered by extended (long) open path (OP) geometries, using an FTIR spectrometer and IR source separated by potentially hundreds of meters and positioned such that the advected plume passes through the optical path. Whilst commonly deployed in studies of ambient and polluted air, industrial and volcanic emissions (e.g., Gosz et al., 1998; Hren et al., 2000; Bacsik et al., 2006; Oppenheimer and Kyle, 2007) extended OP-FTIR seems not to have been exploited at sites of open vegetation fires since the first demonstration by Griffith et al. (1991). Fernández-Gómez et al. (2011) suggest the time is right for a re-appraisal of the approach, and here we use an extended OP-FTIR setup to measure multiple gases emitted from African savannah burns rapidly, simultaneously and without problems of wall loss or chemical conversion, probing cross-sections of individual smoke plumes in a way somewhat similar aircraft sampling.

ACPD
11, 3529–3578, 2011

3 Methodology

3.1 Study area

We analyse the smoke from four prescribed burns conducted in August 2007 – referred to here as Fires 1 to 4. Fires were conducted in Kruger National Park (KNP), South Africa, whose recent fire history is detailed in Archibald et al. (2010). Fires were perimeter ignition events conducted towards the peak of the Southern Africa fire season at the KNP long-term experimental burn plots, detailed in Govender et al. (2006). These 7 ha (380 m×180 m) plots were previously used for emissions studies by Ward et al. (1996), and each had its fuel characteristics and consumption measured via in situ destructive sampling (Table 1). Each plot was first ignited with a backfire (in part to create a larger fire break at the downwind side), followed by headfire ignition some minutes later at the upwind side. Flaming combustion usually ceased when the headfire reached the downwind plot boundary and/or the area already burnt out by the backfire, typically around 30 min after ignition. On some plots substantial residual smouldering combustion (RSC) continued for tens of minutes after all flaming activity ceased. Meteorological conditions were logged throughout each burn.

3.2 FTIR measurements

IR spectra were collected using an OP-FTIR Air Monitoring System (MIDAC Corporation, Irvine CA), equipped with a 76 mm Newtonian telescope to deliver a ~9-mrad field-of-view and deployed neighbouring each burning plot as shown in Fig. 1. A Stirling-cycle cooled mercury-cadmium-telluride (MCT) detector sensitive over the SWIR to TIR spectral range was used to avoid the requirement for liquid nitrogen in the field. The cooled detector, instrument electronics and spectrometer mechanical assemblage were encased in a light, sheet metal casing (size=356×183×166 mm; mass ~9.5 kg) powered by a 12 V battery and controlled by a laptop computer through a dedicated PCMCIA interface. This detection system was tripod mounted at head height and

ACPD
11, 3529–3578, 2011

targeted at a battery powered IR source comprising a tripod-mounted 1275 °C silicon carbide glower located at the focus of a ∼50 cm gold plated aluminium reflector. The spectrometer and IR source were positioned slightly downwind of the plot, and separated by ∼150–250 m such that the horizontally advected plume filled a significant fraction of the intervening path (Fig. 2). Longer optical paths were theoretically possible, but in practice were blocked by trees and undulating terrain. Nevertheless, the extended pathlengths achieved meant that the quantity of smoke being advected into the optical path was sufficient to completely obscure the IR source when viewed with the naked eye from the detector location (as demonstrated in Fig. 1). We recorded raw interferograms (IFGs) at the highest available spectral resolution (0.5 cm^{-1}), with 8 consecutive scans stacked to improve S/N resulting in an 8-s acquisition time step.

3.3 FRP measurements

During each fire, a GPS-equipped helicopter hovered some hundreds of meters above and slightly to the side of each plot, enabling aerial recording of each fire event over the entire plot area. An AGEMA-550 middle infrared (MIR) thermal imager was used to record the fires radiant energy emission signature across a 320×240 pixel imaging array. A narrowband filter centred at 3.9 µm was fitted to prevent detector saturation over high intensity fire pixels. Mean ground pixel size across the 40°×30° field-of-view was 1.5–2.5 m, depending upon flying height, calculated using the viewing distance and angle from the helicopter to the plot as determined from the GPS records. Per-pixel measures of FRP were calculated according to the MIR radiance method of Wooster et al. (2003). For each IR imaging frame, the FRP for each detected fire pixel was summed to provide an instantaneous plot-integrated time-stamped FRP measure. This time-series was generated at 5-s intervals for the entire fire duration. Full details of this processing approach are given in Wooster et al. (2005) and Freeborn et al. (2008). A standard 25 Hz digital video camera was mounted alongside the AGEMA-550 to provide a matching optical video record. Figure 2 includes imagery from both cameras, which was later used in the analysis to track the movement of the active fire front and

ACPD
11, 3529–3578, 2011

smoke plume, and to confirm the timing of the separate combustion stages reported by the ignition team. The backfire and headfire stages of each fire were identified based on the direction of travel of the flaming front in relation to the predominant wind direction, a somewhat similar approach to that previously used to distinguish these stages in satellite imagery (Smith and Wooster, 2005). The RSC stage was simply identified as the period of smoke production after all flaming combustion had ceased.

3.4 Retrieval of trace gas abundances

The co-added IFGs were zero-filled by a factor of 2 and had a Mertz phase correction and triangular apodization function applied prior to conversion to single beam (SB) spectra via a Fourier transform (Smith, 1996). This pre-processing was enacted in the AutoQuant Pro control and analysis software (MIDAC Corporation, Irvine, CA). Figure 3 shows an example of an SB measurement spectrum collected when viewing the IR source horizontally through the smoke, together with a "ambient" spectrum collected without the IR source and which is used to ascertain the contribution of instrument and ambient background emission to the measurement spectra (Müller et al., 1999). Figure 4 shows examples of pre-fire and during-fire SB measurement spectra collected over the spectral window used to retrieve the CO_2 and CO (horizontal) column amounts, with the increased absorption features caused by elevated in-plume abundances clearly apparent.

Trace gases within the plume and the ambient atmosphere were identified directly from their spectral signatures in the recorded SB spectra. Briz et al. (2007) provide a detailed review of the methods available to retrieve trace gas column abundances from OP-FTIR spectroscopy data, concluding that approaches based on spectral forward models maybe effective in removing the need for a clean "background" spectrum and avoiding problems with non-linear departures from the Beer-Lambert Law (Childers, 2001). We use such an approach, described in detail by Burton (1998) and Horrocks et al. (2001). The retrieval algorithm is a combination of the Atmospheric Radiation Reference Forward Model (RFM v4.0 available at www.atm.ox.ac.uk/RFM/; Ed-

ACPD
11, 3529–3578, 2011

wards and Dudhia, 1996), the HITRAN 2008 (and updates) spectral database (a compilation of spectroscopic parameters for 42 atmospheric molecules; Rothman et al., 2009), the optimal estimation procedure of Rodgers et al. (1976), and the enhanced non-linear fitting procedure of Marquardt (1963). The importance of using an up-to-date version of HITRAN was indicated by the fact that testing with HITRAN 1996 produced some emission ratios up to 20% lower than those obtained with the most recent database. These effects should be borne in mind when comparing results from current HITRAN-based FTIR studies to those from prior experiments using older databases.

The retrieval algorithm is parameterized with the atmospheric temperature, pressure, optical path length and the a priori column abundances of the target gases that have absorption features within the spectral window of interest. The transmission of IR radiation along the open path is calculated, and a simulated SB spectrum produced. This output is compared to the measured SB spectrum, and a non-linear least squares fitting routine used to optimize the fit by adjusting the assumed trace gas abundances within the simulation. Being similar in design to the widely used SFIT code (Niple et al., 1980; Benner et al., 1995) and the Multiple Atmospheric Layer Transmission model (MALT; Griffith, 1996), the Burton (1998) code has been used in many studies, in particular of volcanic plumes (e.g., Francis et al., 1998; Burton et al., 2000; Oppenheimer and Kyle, 2007). It has been evaluated by Horrocks et al. (2001) to have an absolute accuracy of better than 5%, with the uncertainty in the HITRAN spectral line parameters determined to be of a similar magnitude. Yokelson et al. (1996) and Smith et al. (2011) calculated similar accuracies for MALT-based trace gas retrievals during closed-path FTIR studies of both real and simulated biomass burning emissions.

The focus of our work was retrieval of the primary carbonaceous species emitted preferentially during the flaming (CO_2), smoldering (CO, CH_4) and pyrolysis (CH_2O) fires phases, but we also searched the IR spectra for signs of nitrogenous compounds. N_2O could also not be readily detected above background levels, in agreement with other findings (e.g., Griffith et al., 1991). Absorption features for NO (around 1900 cm^{-1}) and NO_2 (around 2920 cm^{-1}) were detectable in some but not all of the

ACPD
11, 3529–3578, 2011

SB spectra, most commonly those measured during periods of higher trace gas column amount. Ammonia, a nitrogenous species emitted primarily in the smouldering phase, was the most readily detected N species, in apparent agreement with Griffith et al. (1991) and Yokelson et al. (1997), and we therefore retrieved NH_3 column amounts from all measured spectra. Table 2 lists the spectral windows used for retrieval of each trace gas, where the trace gas(es) of interest possess significant but unsaturated absorption features and where there is limited interference from other species. The "ambient emission" spectrum in Fig. 3, collected without the IR source, confirms that in the higher wavenumber (i.e., shorter wavelength) spectral regions used to retrieve CO_2, CO, CH_4 and CH_2O the signal contribution from instrument self-emission and other ambient temperature sources is minor. Our calculations confirm its effect can be neglected in the retrieval of trace gas column amounts (Müller et al., 1999). However, the lower wavenumber region used to retrieve NH_3 lies in the peak spectral emission region for ambient temperature bodies, and Fig. 3 confirms a substantial "ambient" signal at these sub-1000 cm^{-1} wavenumbers. This signal component needs to be removed from the measurement spectra prior to any trace gas retrieval, since it contains no information on smoke trace gas absorption. We therefore subtracted a relevant ambient SB spectrum from each measurement spectrum, making slight adjustments for MCT detector non-linearities according to Müller et al. (1999) to ensure the resultant "difference" spectrum showed zero signal in spectral regions expected to be fully opaque, such as the 668–670 cm^{-1} CO_2 absorption band (Fig. 3 inset).

Figure 4 demonstrates the high quality of the match between our best-fit forward modeled spectral signal and the measured SB spectra, both prior to and during the fire (i.e., "clean air" and "smoke polluted air"). A full error analysis for the Burton (1998) retrieval approach can be found in Horrocks et al. (2001). The FTIR-derived ambient CO_2 mixing ratio of 413±6 µmol mol^{-1} (mean±1 s d) calculated on a dry air basis before Fire 1 from 5 min of 8 s temporal resolution spectrometer data compares reasonably well to the 417±1 µmol mol^{-1} measure provided by a newly calibrated LICOR IR Gas Analyser. The degree of agreement is of the same order to that found previously by

ACPD
11, 3529–3578, 2011

Yokelson et al. (1997) using a similar forward modeling approach. Pre-fire retrievals for the other species examined here were also found to be reasonable.

3.5 Determination of derived trace gas plume metrics

Forward modeling of the measured IR spectra provides the total number of molecules of the target gas species (x) per unit area along the horizontal observation pathlength (molecules cm^{-2}), here termed the "column amount". This metric represents the integration of the species abundance in molecules per unit volume along the optical pathlength (l, m). The optical pathlength between the IR source and spectrometer was carefully measured, but the helicopter video record confirms that for most of the fires' duration only a fraction of the path (f) was filled by plume (see Fig. 2). Therefore the retrieved column amount represents a mixture of ambient air and smoke in unknown relative quantities. Nevertheless, since for each fire the optical path (l) remains constant, the retrieved column amounts do represent the relative proportions of each trace gas present along the path and can thus be used to determine the smoke plume emission ratios, emissions factors and MCE, as detailed below.

3.5.1 Emission Ratios (ERs)

The smoke emission ratio [$ER_{x/y}$] is commonly defined from the gradient of the linear best fit to the excess abundance of trace gas species (x) when plotted against that of reference species (y) (Yokelson et al., 1999). CO_2 is commonly the reference species for "flaming dominant" compounds, and CO for "smoldering dominant" (Andreae and Merlet, 2001). Where ambient reference species concentrations are difficult to obtain, for example where the background air is suspected to already be fire-affected, Guyon et al. (2005) recommend using the gradient of the absolute gas mixing ratios rather than their excess abundances, an approach adopted by Keene et al. (2006). Furthermore, since in our OP-FTIR approach the smoke plume typically only partly fills the optical path, the number of molecules of species (x) and (y) present in the horizontal measurement column is a weighted average of the amounts in the plume and ambient atmosphere (Horrocks, 2001):

ACPD
11, 3529–3578, 2011

$$x = lf[X_p] + l(1-f)[X_a] \quad (1)$$

$$y = lf[Y_p] + l(1-f)[Y_a] \quad (2)$$

where $[X_p]$ and $[Y_p]$ are, respectively, the mean molecular volumetric abundances of species (x) and (y) in the pure plume, and $[X_a]$ and $[Y_a]$ are the volumetric abundances of the same species in the pure ambient atmosphere (all expressed in units of molecules cm^{-3}); and (x) and (y) are, respectively, the total column amounts of these species measured along the optical path (in units of molecules cm^{-2}); l is the pathlength (here expressed in cm) and f the unitless fraction of the optical path taken up by the pure plume.

Subtracting pre-fire "ambient" abundances from those derived from the during-fire measurements in order to calculate the excess trace gas amounts is therefore not fully correct, since only fraction $(1-f)$ of the optical path contains "clean" air. Fortunately Eqs. (1) and (2) can be combined to remove dependence on the unknown and variable f:

$$y = \left(\frac{Y_p - Y_a}{X_p - X_a}\right) x - l\left[X_a\left(\frac{Y_p - Y_a}{X_p - X_a}\right) - Y_a\right] \quad (3)$$

Equation (3) is effectively the equation of a straight line ($y=mx+c$) obtained when the column amount of species (y) is plotted against that of species (x), where the gradient (m) is a function of the relative abundance of the two species in the "pure" plume and "pure" atmosphere:

$$m = \left(\frac{Y_p - Y_a}{X_p - X_a}\right) \quad (4)$$

Under the assumption that volumetric abundances of the target species in the pure "unmixed" plume are much greater than those in the pure ambient atmosphere (i.e., $Y_p \gg Y_a$ and $X_p \gg X_a$) then m approaches that of the molar emissions ratio of the pure

ACPD
11, 3529–3578, 2011

plume (i.e., $ER_{x/y}=Y_p/X_p$). Gases having both high in-plume abundances (CO_2~90% and CO~6% on a dry air basis according to Andreae and Merlet, 2001) and relatively low in-plume abundances (CH_4~0.3% and NH_3~0.04%) exist in amounts orders of magnitude greater than in the ambient atmosphere, making the gradient (m) equivalent to that of the pure plume ER to within 1%. Hence, as with volcanic plumes (e.g., Sawyer et al., 2008), we can confidently proceed to calculate ERs directly from the retrieved total column amounts.

$ER_{x/y}$ can vary substantially between different phases, resulting in divergent gradients in the (x) vs. (y) column amount scatter plots (e.g., see examples in Fernández-Gómez et al., 2011) . Thus phase-specific emission ratios are often calculated, and to calculate the "fire averaged" emission ratio, either the entire amount of species (x) and (y) released in each phase must be measured and ratioed, which is achievable in laboratory studies, but impossible for most field setups. Alternatively the weighted average of the instantaneous or phase-specific $ER_{x/y}$ measures can be calculated using the relative amount of fuel consumed in the relevant time interval. Such fuel consumption data are again relatively easily obtained during laboratory-scale measurements, but are usually unavailable in field situations. However, in the current study the Fire Radiative Energy (FRE) data derived from temporal integration of the helicopter-born FRP observations can provide this information. This is because FRE is linearly proportional to fuel consumption, irrespective of whether the fire activity is flaming or smouldering, providing the emitter temperature exceeds ~700 K (Wooster et al., 2003, 2005). It should be noted that whilst the FRE measurements are associated with combustion occurring across the entire plot, the trace gas abundances did not always encompass the full plume width due to the optical path not extending along the complete ~380 m plot length. Nevertheless, careful inspection of the aerial video record suggests that the optical paths used were appropriate to effectively sample large parts of the plume from each stage of each fire. When calculating "fire averaged" ERs via weighting of the individual stage ERs by the relevant FRE value, we therefore rely on our "plume integrated" trace gas measures being representative of the entire plume width.

ACPD
11, 3529–3578, 2011

3.5.2 Emission Factors (EFs)

Following Yokelson et al. (1999), Goode et al. (2000), Sinha et al. (2003a) and others, we calculate the emissions factor for species (x) using the carbon mass balance method of Ward and Radke (1993):

$$\mathrm{EF}_x = F_c 1000 \frac{\mathrm{MM}_x}{\mathrm{MM}_{\mathrm{carbon}}} \frac{C_x}{C_T} \quad (5)$$

Where EF_x is the emissions factor for species x ($\mathrm{g\,kg^{-1}}$), F_c is the mass fraction of carbon in the fuel (taken here as 0.5±0.05 to be compatible with the majority of other studies; Ward et al., 1996), MM is the molecular mass of species x (g), 1000 g/kg is a unit conversion factor, $\mathrm{MM}_{\mathrm{carbon}}$ is the molecular mass of carbon (12 g), and C_x/C_T is the ratio of the number of moles of species x in the plume divided by the total number of moles of carbon, calculated as:

$$\frac{C_x}{C_T} = \frac{\mathrm{ER}_{x/\mathrm{CO_2}}}{\sum_{j=1}^{n} (\mathrm{NC}_j \mathrm{ER}_{j/\mathrm{CO_2}})} \quad (6)$$

Where NC_j is the number of carbon atoms in compound j and the sum is over all carbonaceous species, including $\mathrm{CO_2}$.

As is typical in past studies, not all carbon containing species were quantified in our analysis. Delmas et al. (1995) and Keene et al. (2006) show that $\mathrm{CO_2}$ and CO account for the vast majority of the total carbon flux from open biomass burning, a median of around 99% in the case of Southern African savannah fires. The majority of the remaining carbon is emitted as aerosols, and Yokelson et al. (1999) suggest that EFs are underestimated by only 1 or 2% when neglecting these particulates. The carbonaceous gases studied here ($\mathrm{CO_2}$, CO, $\mathrm{CH_4}$ and $\mathrm{CH_2O}$) therefore clearly represent almost the total mass of carbon released, and unmeasured trace gases and particulates are ignored, which inflates the derived EFs by a few percent at most (Yokelson et al., 1999; Andreae and Merlet, 2001; Goode et al., 2000).

ACPD
11, 3529–3578, 2011

3.5.3 Modified Combustion Efficiency (MCE)

The MCE represents the molar ratio of carbon emitted in the form of CO_2 to that emitted as CO and CO_2 (Ward and Radke, 1993):

$$\mathrm{MCE} = \frac{\Delta CO_2}{(\Delta CO_2 + \Delta CO)} \quad (7)$$

where ΔCO_2 and ΔCO indicate the excess mixing ratio of those species (Ward and Radke, 1993). Linear relationships between species EF_x and MCE were used by Goode et al. (2000) to propose a mechanism to estimate the EFs of unmeasured species in cases where CO and CO_2 measures are available, thus highlighting the potential importance of the MCE measure. Our data in theory allow the MCE (and indeed also ERs) to be derived at a very high temporal resolution (i.e., from each SB spectral measurement), though for this it is necessary to base the calculation on excess trace gas abundances rather than the total trace gas column amounts. The MCE for each fire stage can be also be calculated via the relevant ER_{CO/CO_2} measure using:

$$\mathrm{MCE} = \frac{1}{(1 + ER_{CO/CO_2})} \quad (8)$$

In this work we simply use the MCE measures derived from Eq. (8) as an aid to the interpretation of fire behaviour, rather than to derive other quantities or to separate the individual combustion phases or stages.

4 Results and discussion

4.1 Trace gas and FRP time series

Figure 5 shows the time-series of trace gas column amounts, FRP, MCE and remotely measured fire IR brightness temperature for Fire 1. The shape of the trace gas evolution is broadly similar for each species and approximately matches that of FRP, albeit

ACPD
11, 3529–3578, 2011

shifted a little temporally as the smoke takes time to travel from the main source location (e.g., the fire front) into the OP-FTIR optical path, whereas the overhead AGMEA-550 instantaneously registers the fires thermal radiation release. This small temporal offset has no direct impact on our analysis, since the FRP and trace gas abundances are never compared on an instantaneous basis. The peaks in the trace gas and FRP records do, however, have different relative magnitudes since the proportion of the OP-FTIR optical path filled by plume varies over the fire's lifetime (see Sect. 3.5). Records from the ignition team and study of the optical and thermal video records confirm that the initial, narrower pulse of plume and FRP seen in Fig. 5 (peaking at ~17 min) result from the backfire activity alone, whilst the later, wider pulse (peaking at ~23 min) is dominated by the subsequently ignited headfire. The headfire of Fire 1 was recorded as having extinguished at the downwind end of the plot 39 min after the start of the record shown in Fig. 5, though some FRP and substantial smoke continued to be released for many minutes thereafter and we take this as our RSC sample. Somewhat similar patterns are seen in the data for each of the four fires conducted, though no FRP observations are available for Fire 4 due to difficulties with the AGEMA-550.

4.2 Emission ratios

Molar emissions ratios were determined as described in Sect. 3.5.1. As an example, Fig. 6 shows a series of trace gas species column amounts plotted against those of CO_2 and CO for examples of the three separate fire stages. The least squares linear best-fits are shown in each case, with the gradient taken as the emissions ratio [ER_{X/CO_2} or $ER_{X/CO}$] and the 95% confidence limits on the gradient providing an estimate of the emissions ratio uncertainty. Comparison of these ratios to those calculated via first converting the FTIR-determined column amounts to the equivalent excess molar abundances (as per Sinha et al., 2003a) confirmed differences of less than 1%. Emissions ratios of each targeted species to both CO_2 and CO were assessed in this way, and Table 3 details results for all fires, with a histogram of these data shown in Fig. 7 for easy intercomparison. As is commonly the case (Andreae and Merlet, 2001)

ACPD
11, 3529–3578, 2011

for many gases there was usually a somewhat better correlation to CO than to CO_2 (expected due to their common preferential production during smouldering activity), but the ER_{x/CO_2} ratio was nevertheless derived since it is required for later derivation of emissions factors (via Eqs. 5 and 6). Following Sinha et al. (2003a) we use the strength of the coefficient of determination (r^2) between the abundance of a particular gas species and that of CO or CO_2 to confirm the emissions ratio for that gas as well determined. Most had r^2>0.7, and those species for which the coefficient of determination fell below 0.4 are assumed to be poorly determined and are not shown. In particular the RSC Stage of Fire 2 generated low trace gas column amounts (three orders of magnitude lower than some other fires) from which meaningful ERs could not be calculated. This is confirmed by the photographs shown in Fig. 8, which demonstrate how Fire 2 failed to generate a significant "smoking zone" behind the advancing headfire. Lacaux et al. (1996) characterised a typical headfire plume as containing emissions from both the flaming front and a "smoking" zone located immediately behind, but since Fire 2 generated only a very weak smoking zone, emissions production in the subsequent RSC stage would be expected to be similarly low.

Overall, our results confirm that in most cases emission ratios to CO_2 (i.e., ER_{x/CO_2}) for CO, CH_4 and NH_3 are notably higher during the RSC stage as compared to the flaming stages, whereas those of CH_2O are less so. Emission ratios to CO are also in general somewhat higher for CH_4 and NH_3 during the RSC stage than during the flaming stages, but the reverse is true for CH_2O. Results for Fire 1 appear to follow these trends less clearly than those of the other fires, for reasons discussed below. The contrasting relationships shown for formaldehyde are interpreted to result from its higher production during the pyrolysis phase, thus providing more limited opportunities for its creation during the RSC stage where flaming activity is absent (Koppmann et al., 2005).

Lacaux et al. (1996) provide one of the only prior studies to compare savannah headfire and backfire ERs, measured using a CO and CO_2 analyser deployed at fires including those conducted on the KNP plots. The arithmetic mean of the headfire

ACPD
11, 3529–3578, 2011

ER_{CO/CO_2} values determined for different savannah fires by Lacaux et al. (1996) varied over a $(4.0–12.8)\times10^{-2}$ range, rather similar to the $(6.2–12.3)\times10^{-2}$ range found here. However, when Lacaux et al. (1996) weighted their separate ER measures for the headfire flaming and smoking zones by an estimate of the amounts of fuel believed to have been consumed in each (an assumed ratio of 9:1, respectively) they obtained lower ER_{CO/CO_2} values $(3.0\text{-}5.8)\times10^{-2}$. The backfire ER_{CO/CO_2} range of $(3.4–7.0)\times10^{-2}$ determined by Lacaux et al. (1996) is also lower than the $(5.9–11.4)\times10^{-2}$ range determined here. Lacaux et al. (1996) concluded that headfire and backfire ER_{CO/CO_2} are quite comparable, a finding that our results generally confirm. Unlike Cofer et al. (1996) who suggest ER_{CO/CO_2} of flaming and smouldering combustion for KNP fires to be within a few percent of one another, our results suggest substantial differences can occur. Lacaux et al. (1996) determined smouldering stage ER_{CO/CO_2} to vary over a $(12.1–20.8)\times10^{-2}$ range, similar to the $(9.5–22.4)\times10^{-2}$ range found here and certainly more different to the flaming stage ER_{CO/CO_2} than suggested by Cofer et al. (1996).

Our results for Fire 1 depart somewhat from those of the other fires, in particular in having a ER_{CO/CO_2} that is similar for all three fire stages (headfire, backfire and RSC). A possible cause maybe the large amount of (primarily elephant) dung present in the interior of the Fire 1 burn plot, which was not seen on any other plot and which continued to burn for a long time after passage of the flaming front (Fig. 8c), thus contributing substantially to smoking zone emissions in all three fire stages. Crockett and Engle (1999) show that burning of (North American Bison) dung ignited by grassfires can continue for very substantial periods after the flaming front has passed, and that the resultant combustion characteristics are very different to those of the underlying vegetation fuel. Scholes et al. (1996) and Shea et al. (1996) both previously report dung burning at some of the KNP burn plots, and though we did not measure EFs specifically from burning dung, Keene et al. (2006) report that Southern African (cow) dung has an EF_{CO} around twice that of burning grasses, and an EF_{CO_2} around half that of

ACPD
11, 3529–3578, 2011

burning grass. Therefore, dung ER_{CO/CO_2} is close to four times that of grass, and this difference coupled with the extra fuel load provided by dung seems a possible cause of the similar ER_{CO/CO_2} measured across the three fire stages of Fire 1.

The fire averaged emissions ratios, calculated from the separate stage ERs weighted by the relevant FRE data, are also shown in Table 3. Even though the emissions ratio characteristics of the RSC stage can be significantly different to those of the flaming stages, for all fires the vast majority of fuel consumption took place in the headfire and so the "fire averaged" ERs are dominated by the headfire contribution. This suggests that under conditions where FRE or other fuel consumption measurements are unavailable, including at unplanned wildfires, emissions ratio characterisation using smoke emanating from the main fire front and neighbouring smoking zone is likely to be a relatively good representation of the "fire averaged" values, agreeing with the basic conclusions of Cofer et al. (1996).

Comparisons can be made between the ERs determined here and those from prior studies. It should be noted than many species transform as smoke ages, and thus the measurement timing in relation to the causal fire should be carefully considered (Hobbs et al., 2003). Table 3 includes the relevant mean ER_{x/CO_2} values reported by Sinha et al. (2003a) for non-aged fire smoke from similar KNP fires as studied here, but derived via gas chromatography and closed-path airborne FTIR spectroscopy. Comparison to the current results for CO, CH_4 and CH_2O indicates overlap in the estimates derived via the two approaches, despite the very different sampling and measurement approaches applied, further evidence for the validity of our extended open-path remote sensing approach. Our estimates of $ER_{NH_3/CO}$ are, however, substantially greater than those of Sinha et al. (2003a), and potential reasons for this are discussed in the following Section.

4.3 Emissions factors

Calculated emission factors for all four fires, derived from the ERs via the carbon mass balance approach described in Sect. 3.5.2, are listed in Table 4 and graphed in Fig. 9.

ACPD
11, 3529–3578, 2011

Uncertainties were calculated in quadrature from those associated with the trace gas ERs and the ±10% uncertainty in the assumed fuel carbon content. Fire averaged EFs for each species were again calculated by weighting the EFs calculated for each of the three fire stages by the relevant FRE measure. Table 4 also includes the EFs reported for Southern African savannah fires by Sinha et al. (2003a), which they calculated from their measured ERs that are listed in Table 3. Also listed are EFs taken from the SAFARI-92 KNP airborne study of Cofer et al. (1996), EFs from the widely used database of Andreae and Merlet (2001) and updates, and from the SAFARI-92 and SAFARI-2000 campaigns (Ward et al., 1996; Keene et al., 2006, respectively). Our EFs for CO_2 are similar to those of all the past studies, and in particular are very close to the values derived in the most recent study conducted in almost exactly the same KNP area (Sinha et al., 2003a). The same is true for CH_4, but for CO our "fire averaged" mean EF is in general higher than the mean values determined in past works, though still within the range determined by Ward et al. (1996) and Keene et al. (2006).

In contrast to the relatively good agreement between our EFs and those presented by Andreae and Merlet (2001) for the dominant carbonaceous species, we find the EF of formaldehyde to be significantly elevated (by a factor of ~4–8), though their more recent update included in Table 4 lowers the difference somewhat. Our results therefore confirm the findings of Sinha et al. (2003a) and Yokelson et al. (2003) of significant departures from literature values of savannah fire EF_{CH_2O}, a species directly involved in the production of tropospheric ozone. However, unlike these prior works we do not find major differences between KNP NH_3 emission factors and those presented by Andreae and Merlet (2001) and its updates, and indeed our results are closer to the values quoted in Andreae and Merlet than to those of Sinha et al. (2003a). We note that without appropriate subtraction of the ambient emission signal (which Fig. 3 confirms is highly significant at the lower wavenumbers used to retrieve ammonia) our NH_3 column amounts and thus EFs would be underestimated by ~60%. Thus we were careful to utilize the approach of Müller et al. (1999) when retrieving NH_3 column amounts, and rather than ambient background influences the cause of the discrepancy

ACPD
11, 3529–3578, 2011

in EF_{NH_3} maybe the contrasting measurement methodologies used here and by Sinha et al. (2003a) and Yokelson et al. (2003). In particular, Yokelson et al. (2003) identified NH_3 to be the only targeted species whose concentration was noticeably affected by the brief residence time spent in the closed cell used to contain the sample. It was suggested that mean EF_{NH_3} underestimations of 5–20% may result, though underestimations of up to 50% were apparently seen in pre-flight laboratory tests (Yokelson et al., 2003). Our open path method does not suffer from this effect, potentially explaining at least some of the noted difference in EF_{NH_3}. A further contributory factor may come from the work of Keene et al. (2006), who found fuel-specific EF_{NH_3} to differ substantially between the different KNP fuel components, most probably due to differing nitrogen contents. This makes each EF_{NH_3} highly dependent upon the mix of fuels consumed, and suggests potentially high variability across space and time.

4.4 MCE and fire pixel brightness temperature

Since flaming combustion occurs at a higher temperature than smouldering combustion (Lobart and Warnatz, 1993) it has been suggested that fire temperature estimates derived from airborne or spaceborne Earth observation maybe useful in broadly classifying combustion into predominately flaming (i.e., higher MCE) or smouldering (i.e., lower MCE) activity (e.g., Dennision et al., 2006; Zhukov et al., 2006). Since ERs and EFs can clearly vary substantially between these phases, such discrimination may in future be able to enhance emissions estimation procedures. Since both plume MCE and fire pixel brightness temperature (BT) data are available for the headfire and RSC Stages of Fires 1 and 3 we have some opportunity to examine this potential. Our conclusions must be limited however, since without multi-spectral airborne IR data we can examine pixel-integrated BTs only, which are lower than the fires true radiative temperature due to the area of combustion commonly underfilling the imager pixels. This issue is less significant at the small pixel sizes used here, but would preclude such a simple analysis when using satellite-derived IR BT measures. The pixel-integrated BT measures are also likely to be affected by variations in flame depth, soot production

ACPD
11, 3529–3578, 2011

and other fire processes, but nevertheless the final two panels of Fig. 5 do demonstrate that the Fire 1 MCE and BT data do show a degree of temporal similarity. MCE starts at almost 1.0 during the backfire, decreases into the headfire (mean±σ of 0.86±0.06), and falls further during the period of RSC towards the end of the burn (0.76±0.07), indicating a transition from flaming-dominated to completely smouldering combustion. Maximum BT also decreases over the same time interval (headfire 723±66 K vs. RSC 595±47 K) as does, albeit less significantly, mean BT (headfire 541±21 K vs. RSC 512±10 K). Data from Fire 3 confirms this pattern of decreasing MCE and BT as the combustion moves from flaming to increased smouldering, albeit both the MCE and BT values of the different stages are closer than was seen at Fire 1 (MCE: headfire 0.89±0.05 vs. RSC 0.85±0.01; max BT: headfire 595±62 K vs. RSC 555±41 K; mean BT: headfire 520±17 vs. RSC 512±18 K).

5 Summary and conclusions

A unique high temporal resolution trace gas and FRP dataset has been collected for a series of multi-hectare fires conducted in Kruger National Park, South Africa using extended OP-FTIR spectroscopy operated over 150–250 m pathlengths. These measurements were supplemented by airborne optical and thermal imaging. Following an early demonstration by Griffith et al. (1991), extended OP-FTIR spectroscopy has been relatively little exploited for vegetation fire plume analysis, but reductions in size and cost, and increases in the performance and availability of Stirling-cooled detector systems, have made such deployments increasingly practicable. Our OP-FTIR setup allowed multiple smoke chemical constituents to be probed simultaneously and at a very high temporal resolution across a large proportion (or even the totality) of the advected plume cross section, avoiding many limitations of point-sampling approaches. Trace gas column amounts were derived from the single beam IR spectra using a spectral forward model coupled to a non-linear least squares fitting approach, avoiding the need for experimentally determined reference spectra. The method is

ACPD
11, 3529–3578, 2011

sufficiently sensitive to detect path-averaged CO mixing ratio variations of around 10 ppbv (0.001 µmol mol^{-1}) across the 150–250 m optical paths used here. The retrieved trace gas column amounts allow for the calculation of emissions ratios (ERs) and emissions factors (EFs) for each stage of the studied fires, and stage-specific fire radiative energy (FRE) measures calculated from airborne IR imagery allowed for the determination of "fire averaged" ERs and EFs using a "weighted-mean" approach. The FRE data indicate that only a few percent of total fuel consumption actually occurs in the RSC stage, so even though ERs and EFs are substantially higher for many compounds in the RSC stage, sampling of headfire activity alone actually maybe sufficient for the general assessment of "fire averaged" ERs and EFs in the field, at least in this savannah environment. There therefore appears to be only a limited requirement for concurrent airborne thermal imager observations in campaigns targeting the determination of emissions ratios and emissions factors using OP-FTIR methods, at least in environments with relatively insignificant amounts of burning of organic litter and soil layers.

We focused on a set of key compounds related preferentially to the pyrolysis (CH_2O), flaming (CO_2) and smoldering (CO, CH_4, NH_3) combustion phases. We find ERs for headfires and backfires to be similar, and generally rather different that those seen in the residual smouldering combustion (RSC) stage, apart from at one fire where burning elephant dung appears to have contributed substantially to the emissions characteristics. With CO_2 as the reference species, ERs from the residual smouldering combustion stage are otherwise notably higher than for the flaming stages. Apart from for ammonia, our mean fire averaged ERs lie relatively close to those calculated previously by Sinha et al. (2003a) via airborne sampling in the same study area, though are generally a little higher (by up to 33%; see last rows of Table 3). CO_2 and CH_4 emissions factors derived from the relevant emission ratios show good agreement with those of other studies, including Andreae and Merlet (2001) and subsequent updates. Our EF for carbon monoxide is, however, somewhat higher (by ~45–85%) than the average quoted in most other studies, but still within the range of previous measurements (e.g.,

ACPD
11, 3529–3578, 2011

Keene et al., 2006; Ward et al., 1996). However, we find the EF of formaldehyde to be very significantly higher than existing estimates, even that of Sinha et al. (2003a). This may point to substantial biases in the total calculated emissions for this species for savannah environments, which will pose problems when comparing such bottom-up (e.g., emissions inventories) and top-down (e.g., satellite-derived column totals) estimates of this trace gas. These effects maybe in part responsible for the low-biased CH_2O emissions estimates reported by Stavrakou et al. (2009) when compared to space-based formaldehyde columns. Finally, we find the EF for ammonia to be closer to that of Andreae and Merlet (2001) than to the lower Sinha et al. (2003a) values.

Our work confirms ground-based, extended OP-FTIR as a practical, rapidly deployable, relatively low cost yet effective means of ER and EF determination for open vegetation fires burning in a manner fully representative of wildfire phenomena. It allows substantial parts of the near-ground smoke column to be rapidly and quantitatively assessed before any physical and chemical "ageing" processes take effect. Though we limited our study to only five chemical species, the measured IR spectra also allow quantification of dozens of other molecules should they be present in significant quantities (Yokelson et al., 1999; Sinha et al., 2003a, 2003b, 2004).

The extended OP-FTIR technique could in future allow study of as-yet poorly characterised combustion situations, such as smouldering peat fires and the night-time chemistry occurring in smoke-filled valleys. One potential limitation is that smoke lofted near vertically into the atmosphere is unavailable for sampling via our measurement geometry. However, the relatively low intensity of these KNP savannah fires prevented development of a strong convection column, and indeed our results generally agree well with those from previous airborne campaigns in the same study area which did sample elevated plumes (Sinha et al., 2003a). However, it is possible that our results maybe influenced by the ability to sample only near-ground portions of the plume, which may mean we under-sampled the smoke emanating from the most intensely burning patches of fuel. This maybe part of the explanation of the higher CO emissions factors obtained here when compared to many other studies.

ACPD
11, 3529–3578, 2011

The inability of our OP-FTIR approach to sample vertically rising plumes will be most important when studying particularly intense fires and/or those in higher fuel load environments such as boreal forests. In such cases, it maybe that the extended OP-FTIR method is best focused on emissions characterisation as part of a multi-layered approach, including aircraft deployments to characterise the higher altitude plume components. It may also be possible to adapt the method to encompass a solar-occultation viewing geometry, an approach which has proven successful in studies of high altitude volcanic plumes (Francis et al., 1998; Duffell et al., 2001) and smoke-polluted atmospheres (e.g., Paton-Walsh et al., 2005, 2008). We concur with Fernández-Gómez et al. (2011), that OP-FIR operated in extended open-path mode at real vegetation fires offers a unique tool for investigating combustion emission dynamics at scales otherwise difficult to probe using alternative ground-based approaches.

Acknowledgements. Financial support for parts of this scientific research came from the European Commission, which funded the project "CarboAfrica" (GOCE, 037132) under the 6th Framework Programme (FP6). Other financial support came from funding to King's College London made to PI Wooster under the NERC National Center for Earth Observation (NCEO). Riccardo Valentini and colleagues of the Laboratory of Forest Ecology, University of Tuscia (Italy) are thanked for support in the field. Antonio Bombelli of the same laboratory provided logistical assistance, and Gerado Fratini the LICOR IR Gas Analyser measures. We are indebted to South African National Parks for their great assistance with many aspects of this study and for access to their data. Bob Scholes (CSIR Natural Resources and the Environment) helped formulate this collaboration and provided invaluable advice in the field. The role of the team that maintained the KNP fire experiment (especially Andre Potgieter) is gratefully acknowledged, as is that of the NERC Field Spectroscopy Facility (FSF), particularly Chris Maclellan and Alasdair Mac Arthur, who procured the OP-FTIR system used here (loaned from NERC FSF) and who provided invaluable advice, support and logistical assistance related to the deployment. Meinrat Andreae is thanked for providing updates to the Andreae and Merlet (2001) EF database. Nathan Wooster and Alec Wooster are thanked for their support and for assistance with OP-FTIR setup evaluation in the UK prior its field deployment. Finally, we are grateful to Georgina Sawyer of the Department of Geography, University of Cambridge (UK) for her advice on FTIR retrieval specifics using the code deployed here, and to Bob Yokelson

ACPD
11, 3529–3578, 2011

of the University of Montana (USA) and an anonymous reviewer for their incisive and detailed comments that helped improve the content and clarity of this manuscript.

References

Andreae, M. O. and Merlet P.: Emission of trace gases and aerosols from biomass burning, Global Biogeochem. Cy., 15, 955–966, 2001.

Archibald, S., Nickless, A., Govender, N., Scholes, R. J., and Lehsten, V.: Climate and the inter-annual variability of fire in Southern Africa: a meta-analysis using long-term field data and satellite-derived burnt area data, Global Ecol. Biogeogr., 19, 794–809, doi:10.1111/j.1466-8238.2010.00568.x2010, 2010.

Bacsik, Z. Viktoria, A., Komlosi, A., Ollar, T., B., and Mink, J.: Comparison of open path and extractive long-path FTIR techniques in detection of air pollutants, Appl. Spectrosc. Rev., 41, 77–97, 2006.

Benner D. C., Rinsland C. P., Devi, V. M., Smith, M. A. H., and Atkins, D.: A multi-spectrum nonlinear least squares fitting technique, J. Quant. Spectropsc. Ra., 53, 705–721, 1995.

Bertschi, I., Yokelson, R. J., Ward, D. E., Babbitt, R. E., Susott, R. A., Goode, J. G., and Hao, W.: Trace gas and particle emissions from fires in large diameter and belowground biomass fuels, J. Geophys. Res., 108(D13), 8472, doi:8410.1029/2002JD002100, 2003.

Bowman, D. M., Balch, J. K., Artaxo, P., Bond, W. J., Carlson, J. M., Cochrane, M. A., D'Antonio, C. M., Defries, R. S., Doyle, J. C., Harrison, S. P., Johnston, F. H., Keeley, J. E., Krawchuk, M. A., Kull, C. A., Marston, J. B., Moritz, M. A., Prentice, I. C., Roos, C. I., Scott, A. C., Swetnam, T. W., van der Werf, G. R., and Pyne, S. J.: Fire in the Earth system, Science, 324, 481–484, 2009.

Briz, S., de Castro, A. J., Diez, S., Lopez, F., and Schafer, K.: Remote sensing by open-path FTIR spectroscopy. Comparison of different analysis techniques applied to ozone and carbon monoxide detection, J. Quant. Spectrosc. Ra., 103, 314–330, 2007.

Burton, M.: Remote Sensing of the Atmosphere Using Fourier Transform Spectroscopy, PhD Thesis, University of Cambridge, Cambridge, UK, 1998.

Burton, M. R., Oppenheimer, C., Horrocks, L. A., and Francis, P. W.: Remote sensing of CO_2 and H_2O emission rates from Masaya volcano, Nicaragua, Geology, 28, 915–918, 2000.

Castro, A. J., Lerma, A. M., López, F., Guijarro, M., Díez, C., Hernando, C., and Madrigal, J.:

ACPD
11, 3529–3578, 2011

Open-path Fourier transform infrared spectrometry characterization of low temperature combustion gases in biomass fuels, Infrared Phys. Techn., 51, 21–30, 2007.
Childers, J. W., Thomson, E. L., Harris, D. B., Kirchgessner, D. A., Clayton, M., Natschke, D. F., and Phillips, W. J.: Multi-pollutant concentration measurements around a concentrated swine production facility using open-path FTIR spectrometry, Atmos. Environ., 35, 1923–1936, 2001.
Christian, T. J., Yokelson, R. J. Carvalho Jr., J. A., Griffith, D. W. T., Alvarado, E. C., Santos, J. C., Neto, T. G. S., Veras, C. A. G., and Hao W. M.: The tropical forest and fire emissions experiment: trace gases emitted by smoldering logs and dung from deforestation and pasture fires in Brazil, J. Geophys. Res., 112, D18308, doi:10.1029/2006JD008147, 2007.
Crockett, J. S. and Engle, D. M.: Combustion characteristics of Bison (Bison Bison) fecal pats ignited by grassland fires, Am. Midl. Nat., 141, 12–18, 1999.
Cofer III, W. R., Levine, J. S., Winstead, E. L., Cahoon, D. R., Sebacher, D. I., Pinto, J. P., and Stocks, B. J.: Source compositions of trace gases released during African savanna fires, J. Geophys. Res., 101, 23597–23602, 1996.
Delmas, R., Lacaux, J. P., and Brocard, D.: Determination of biomass burning emission factors: methods and results, Environ. Monit. Assess., 38, 181–204, 1995.
Dennison, P. E., Charoensiri, K., Roberts, D. A., Peterson, S. H., and Green, R. O.: Wildfire temperature and land cover modeling using hyperspectral data, Remote Sens. Environ., 100, 212–222, 2006.
Duffell, H., Oppenheimer, C., and Burton, M. R.: Volcanic gas emission rates measured by solar occultation spectroscopy, Geophys. Res. Lett., 28, 3131–3134, 2001.
Edwards, D. J. and Dudhia, A.: Reference Forward Model: High Level Algorithms Definition, ESA Doc. POMA-OXF-GS-0004, European Space Agency, Paris, 1996.
Francis, P., Burton, M., and Oppenheimer, C.: Remote measurements of volcanic gas compositions by solar FTIR spectroscopy, Nature, 396, 567–570, 1998.
Freeborn, P. H., Wooster, M. J., Hao, W. M., Ryan, C. A., Nordgren, B. L., Baker, S. P., and Ichoku, C.: Relationships between energy release, fuel mass loss, and trace gas and aerosol emissions during laboratory biomass fires, J. Geophys. Res., 113, D01102, doi:10.1029/2007JD008489, 2008.
Freeborn, P. H., Wooster, M. J., Roberts, G., Malamud, B., and Xu, W.: Development of a virtual active fire product for Africa through a synthesis of geostationary and polar orbiting satellite data, Remote Sens. Environ., 113, 1700–1711, 2009.

ACPD
11, 3529–3578, 2011

Fernández-Gómez, I., de Castro, A. J., Guijarro, M., Madrigal, J., Aranda, J. M., Diez, C., Hernando, C., and Lopez, F.: Characterization of forest fuels in a mass loss calorimeter by short open-path FTIR spectroscopy, J. Quant. Spectrosc. Ra., 112, 519–530, 2011.

Giglio, L., Loboda, T., Roy, D. P., Quayle, B., and Justice, C. O.: An active-fire based burned area mapping algorithm for the MODIS sensor, Remote Sens. Environ., 113, 408–420, 2009.

Goode, J. G., Yokelson, R. J., Susott, R. A., and Ward, D. E.: Trace gas emissions from laboratory biomass fires measured by open-path FTIR: fires in grass and surface fuels, J. Geophys. Res., 104, 21237–21245, 2000.

Gosz, J. R., Clifford, N. D., and Risser, P. G.: Long-path FTIR measurement of atmospheric trace gas concentrations, Ecology, 69, 1326–1330, 1988.

Govender, N., Trollope, W. S. W., and van Wilgen, B. W.: The effect of fire season, fire frequency, rainfall and management on fire intensities in savanna vegetation in South Africa, J. Appl. Ecol., 43, 748–758, 2006.

Griffith, D.: Synthetic calibration and quantitative analysis of gas-phase FT-IR spectra, Appl. Spectrosc., 50, 59–70, 1996.

Griffith, D. W. T., Mankin, W. G., Coffey, M. T., Ward, D. E., and Reibau, A.: FTIR remote sensing of biomass burning emissions of CO_2, CO, CH_4, CH_2O, NO, NO_2, NH_3 and N_2O, in: Global Biomass Burning: Atmospheric, Climatic, and Biospheric Implications, edited by: Levine, J., MIT Press, Cambridge, Mass, 230–240, 1991.

Guyon, P., Frank, G. P., Welling, M., Chand, D., Artaxo, P., Rizzo, L., Nishioka, G., Kolle, O., Fritsch, H., Silva Dias, M. A. F., Gatti, L. V., Cordova, A. M., and Andreae, M. O.: Airborne measurements of trace gas and aerosol particle emissions from biomass burning in Amazonia, Atmos. Chem. Phys., 5, 2989–3002, doi:10.5194/acp-5-2989-2005, 2005.

Hobbs, P. V., Sinha, P., Yokelson, R. J., Christian, T. J., Blake, D. R., Gao, S., Kirchstetter, T. W., Novakov, T., and Pilewskie, P.: Evolution of gases and particles from a savanna fire in South Africa, J. Geophys. Res., 108(D13), 8485, doi:10.1029/2002JD002352, 2003.

Horrocks, L.: Infrared Spectroscopy of Volcanic Gases at Masaya, Nicaragua, PhD Thesis, Open University, Milton Keynes, UK, 253 pp., 2001.

Horrocks, L. A., Oppenheimer, C., Burton, M. R., Duffell, H. J., Davies, N. M., Martin, N. A., and Bell, W.: Open-path Fourier transform infrared spectroscopy of SO2: An empirical error budget analysis, with implications for volcano monitoring, J. Geophys. Res., 106, 27647–27659, doi:10.1029/2001JD000343, 2001.

Hren, B., Katona, K., Mink, J., Kohán J., and Isaák, G. Y.: Long-path FTIR spectroscopic studies

ACPD
11, 3529–3578, 2011

of air pollutants in the Danube refinery plant, Analyst, 125, 1655–1659, 2000.
Kaiser, J., Boucher, O., Doutriaux-Boucher, M., Flemming, J., Govaerts, Y. M., Gulliver, J., Heil, A., Jones, L., Lattanzio, A., Morcrette, J.-J., Perrone, M. R., Razinger, M., Roberts, G., Schultz, M. G., Simmons, A. J., Suttie, M., and Wooster, M. J.: Smoke in the Air, ECMWF Newsletter, 119, available at: http://www.ecmwf.int/publications/newsletters/ (last access: December 2010), 2009.
Keene, W. C., Lobert, J. M., Crutzen, P. J., Maben, J. R., Scharffe, D. H., and Landmann, T.: Emissions of major gaseous and particulate species during experimental burns of Southern African biomass, J. Geophys. Res., 108, D04301, doi:10.1029/2002JD002352, 2006.
Koppmann, R., von Czapiewski, K., and Reid, J. S.: A review of biomass burning emissions, part I: gaseous emissions of carbon monoxide, methane, volatile organic compounds, and nitrogen containing compounds, Atmos. Chem. Phys. Discuss., 5, 10455–10516, doi:10.5194/acpd-5-10455-2005, 2005.
Korontzi, S., Ward, D. E., Susott, R. A., Yokelson, R. J., Justice, C. O., Hobbs, P. V., Smithwick, E. A. H., and Hao, W. M.: Seasonal variation and ecosystem dependence of emission factors for selected trace gases and PM for Southern African savanna fires, J. Geophys. Res., 108(D24), 4758, doi:10.1029/2003JD003730, 2003.
Korontzi, S., Roy, D. P., Justice, C. O., and Ward, D. E.: Modeling and sensitivity analysis of fire emissions in Southern Africa during SAFARI 2000, Remote Sens. Environ., 92, 376–396, 2004.
Lacaux, J.-P., Delmas, R., Jambert, C., and Kuhlbusch, T. A. J.: NO_x emissions from African savanna fires, J. Geophys. Res., 101, 23585–23596, 1996.
Lobart, J. M. and Warnatz, J.: Emissions from the combustion processes in vegetation, in: Fire in the Environments: The Ecological, Atmospheric, and Climatic Importance of Vegetation Fires, edited by: Crutzen, P. J., Goldammer, J. G., John Wiley and Sons, New York, 1993.
Marquardt, D. W.: An algorithm for least squares estimation of non-linear problems, J. Soc. Ind. Appl. Math., 11, 431–441, 1963.
Müller, U., Kurte, R., and Heise, H. M.: Investigation of photometric errors in FTIR-spectra obtained in open-path monitoring, J. Mol. Struct., 482–483, 539–544, 1999.
Niple, E.: Non linear least squares analysis of atmospheric absorption spectra, Appl. Optics, 19, 3481–3490, 1980.
Oppenheimer, C. and Kyle, P. R.: Probing the magma plumbing of Erebus volcano, Antarctica, by open-path FTIR spectroscopy of gas emissions, J. Volcanol. Geoth. Res., 1, 743–754,

ACPD
11, 3529–3578, 2011

2007.
Paton-Walsh, C., Jones, N. B., Wilson, S. R., Haverd, V., Meier, A., and Griffith, D. W. T.: Measurements of trace gas emissions from Australian forest fires and correlations with coincident measurements of aerosol optical depth, J. Geophys. Res., 110, D24305, doi:10.1029/2005JD006202, 2005.
Paton-Walsh, C., Wilson, S. R., Jones, N. B., and Griffith, D. W. T.: Measurement of methanol emissions from Australian wildfires by ground-based solar Fourier transform spectroscopy, Geophys. Res. Lett., 35, L08810, doi:10.1029/2007GL032951, 2008.
Reid, J. S., Hyer, E. J., Prins, E. M., Westphal, D. L., Zhang, J., Wang, J., Christopher, S. A., Curtis, C. A., Schmidt, C. C., Eleuterio, D. P., Richardson, K. A., and Hoffman, J. P.: Global monitoring and forecasting of biomass-burning smoke: description of and lessons from the forecasting and modeling of burning emissions (FLAMBE) program, IEEE Sel. Top. Appl. Earth Observ. Remote Sens., 34, 144–162, 2009.
Roberts, G., Wooster, M. J., and Lagoudakis, E.: Annual and diurnal african biomass burning temporal dynamics, Biogeosciences, 6, 849–866, doi:10.5194/bg-6-849-2009, 2009.
Rodgers, C. D.: Retrieval of atmospheric temperature and composition from remote measurements of thermal radiation, Rev. Geophys. Space Phys., 14, 609–624, 1976.
Rothman, L. S., Gordon, I. E., Barbe, A., Chris Benner, D., Bernath, P. F., Birk, M., Boudon, L. V., Brown, R., Campargue, A., Champion, J.-P., Chance, K., Coudert, L. H., Dana, V., Devi, V. M., Fally, S., Flaud, J.-M., Gamache, R. R., Goldman, A., Jacquemart, D., Kleiner, I., Lacome, N., Lafferty, W. J., Mandin, J.-Y., Massie, S. T., Mikhailenko, S. N., Miller, C. E., Moazzen-Ahmadi, N., Naumenko, O. V., Nikitin, A. V., Orphal, J., Perevalov, V. I., Perrin, A., Predoi-Cross, A., Rinsland, C. P., Rotger, M., Simeckova, M., Smith, M. A. H., Sung, K., Tashkun, S. A., Tennyson, J., Toth, R. A., Vandaele, A. C., and Vander Auwera, J.: The HITRAN 2008 molecular spectroscopic database, J. Quant. Spectrosc. Ra., 110, 533–572, 2009.
Roy, D. P., Boschetti, L., Justice, C. O., and Ju, J.: The collection 5 MODIS burned area product – global evaluation by comparison with the MODIS active fire product, Remote Sens. Environ., 112, 3690–3707, 2008.
Sawyer, G. M., Carn, S. A., Tsanev, V. I., Oppenheimer, C., and Burton, M.: Investigation into magma degassing at Nyiragongo volcano, Democratic Republic of the Congo, Geochem. Geophys. Geosyst., 9, Q02017, doi:10.1029/2007GC001829, 2008.
Scholes, R. J., Ward, D. E., and Justice, C. O.: Emissions of trace gases and aerosol particles

ACPD
11, 3529–3578, 2011

due to vegetation burning in Southern Hemisphere Africa, J. Geophys. Res., 101, 23677–23682, doi:10.1029/95JD02049, 1996.
Shea, R. W., Shea, B. W., Kauffman, J. B., Ward, D. E., Haskins, C. I., and Scholes, M. C.: Fuel biomass and combustion factors associated with fires in savanna ecosystems of South Africa and Zambia, J. Geophys. Res., 101(D19), 23551–23568, doi:10.1029/95JD02047, 1996.
Sinha, P., Hobbs, P. V., Yokelson, R. J., Bertschi, I. T., Blake, D. R., Simpson, I. J., Gao, S., Kirchstetter, T. W., and Novakov, T.: Emissions of trace gases and particles from savanna fires in Southern Africa, J. Geophys. Res., 108, 8487, doi:10.1029/2002JD002325, 2003a.
Sinha, P., Hobbs, P. V., Yokelson, R. J., Blake, D. R., Gao, S., and Kirchstetter T. W.: Distributions of trace gases and aerosols during the dry biomass burning season in Southern Africa, J. Geophys. Res., 108(D17), 4536, doi:10.1029/2003JD003691, 2003b.
Sinha, P., Hobbs, P. V., Yokelson, R. J., Blake, D. R., Gao, S., and Kirchstetter, T. W.: Emissions from miombo woodland and dambo grassland savanna fires, J. Geophys. Res., 109, D11305, doi:10.1029/2004JD004521, 2004.
Smith, B. C.: Fundamentals of Fourier Transform Infrared Spectroscopy, CRC Press, Florida, USA, 205 pp., 1996.
Smith, A. M. S. and Wooster, M. J.: Remote classification of head and backfire types from MODIS fire radiative power observations, Int. J. Wildland Fire, 14, 249–254, 2005.
Smith, T. E. L., Wooster, M. J., Tattaris, M., and Griffith, D. W. T.: Absolute accuracy and sensitivity analysis of OP-FTIR retrievals of CO_2, CH_4 and CO over concentrations representative of "clean air" and "polluted plumes", Atmos. Meas. Tech., 4, 97–116, doi:10.5194/amt-4-97-2011, 2011.
Stavrakou, T., Müller, J.-F., De Smedt, I., van Roozendael, M., van der Werf, G. R., Giglio, L., and Guenther, A.: Evaluating the performance of pyrogenic and biogenic emission inventories against one decade of space-based formaldehyde columns, Atmos. Chem. Phys., 9, 1037–1060, doi:10.5194/acp-9-1037-2009, 2009.
Taylor, J. R.: An Introduction to Error Analysis, University Science Books, Sausalito, CA., 173–180, 1997.
van der Werf, G. R., Randerson, J. T., Collatz, G. J., Giglio, L.: Carbon emissions from fires in tropical and subtropical ecosystems, Global Change Biol., 9, 547–562, 2003.
van der Werf, G. R., Randerson, J. T., Giglio, L., Collatz, G. J., Kasibhatla, P. S., and Arellano Jr., A. F.: Interannual variability in global biomass burning emissions from 1997 to 2004, Atmos. Chem. Phys., 6, 3423–3441, doi:10.5194/acp-6-3423-2006, 2006.

ACPD
11, 3529–3578, 2011

Ward, D. E. and Radke, L. F.: Emission measurements from vegetation fires: a comparative evaluation of methods and results, in: 1993. Fire in the Environment: The Ecological, Atmospheric, and Climatic Importance of Vegetation Fires, edited by: Crutzen, P. J. and Goldammer, J. G., Wiley, Chichester, UK, 53–76, 1993.

Ward, D. E., Hao, W. M., Sussot, R. A., Babbit, R. E., Shea, R. W., Kauffman, J. B., and Justice, C.O.: Effect of fuel composition on combustion efficiency and emission factors for African savanna ecosystems, J. Geophys. Res., 101, 23569–23576, 1996.

Wooster, M. J., Zhukov, B., and Oertel, D.: Fire radiative energy for quantitative study of biomass burning: derivation from the BIRD experimental satellite and comparison to MODIS fire products, Remote Sens. Environ., 86, 83–107, 2003.

Wooster, M. J., Roberts, G., Perry, G., and Kaufman, Y. J.: Retrieval of biomass combustion rates and totals from fire radiative power observations: calibration relationships between biomass consumption and fire radiative energy release. J. Geophys. Res., 110, D24311, doi:10.1029/2005JD006318, 2005.

Xu, W., Wooster, M. J., Roberts, G., and Freeborn, P.: New GOES imager algorithms for cloud and active fire detection and fire radiative power assessment across North, South and Central America, Remote Sens. Environ., 114, 1876–1895, 2010.

Yokelson, R. J., Ward, D. E., Susott, R. A., Reardon, J., and Griffith, D. W. T.: Emissions from smoldering combustion of biomass measured by open-path FTIR, J. Geophys. Res., 102, 18865–18877, 1997.

Yokelson, R. J., Goode, J. G., Ward, D. E., Susott, R. A., Babbitt, R. E., Wade, D. D., Bertschi, I., Griffith, D. W. T., and Hao, W. M.: Emissions of formaldehyde, acetic acid, methanol, and other trace gases from biomass fires in North Carolina measured by airborne Fourier transform infrared spectroscopy, with coincident measurements of aerosol optical depth, J. Geophys. Res., 104, 30109–30126, 1999.

Yokelson, R., Griffith, D., and Ward, D.: Open-path Fourier transform infrared studies of large?scale laboratory biomass fires, J. Geophys. Res., 101(D15), 21067–21080, 1996.

Yokelson, R. J., Bertschi, I. T., Christian, T. J., Hobbs, P. V., Ward, D. E., and Hao, W. M.: Trace gas measurements in nascent, aged, and cloud-processed smoke from African savanna fires 30 by airborne Fourier transform infrared spectroscopy (AFTIR), with coincident measurements of aerosol optical depth, J. Geophys. Res., 108(D13), 8478, doi:10.1029/2002JD002322, 2003.

Zhukov, B., Lorenz, E., Oertel, D., Wooster, M. J., and Roberts, G.: Spaceborne detection and

ACPD
11, 3529–3578, 2011

characterization of fires during the Bi-spectral Infrared Detection (BIRD) experimental small satellite mission 2001–2004, Remote Sens. Environ., 100, 29–51, 2006.

ACPD
11, 3529–3578, 2011

Table 1. Description of the four 7-ha open vegetation fires studied in this work, conducted 27–28 August 2007 at the Kruger National Park experimental burn plots (Govender et al., 2006).

	Plot name	Fuel load fuel consumed (mean±s d; g m^{-2}) fuel moisture (%)	First ignition (local time)	FTIR to IR source distance (m)	Air temp (°C)	RH (%)	Air pressure (mb)	% fuel burned in backfire: headfire: RSC stages
Fire 1	N'was*	184±57 101±82 13.1%	14:01	170	23	23	962	12:87:1
Fire 2	Skukuza	144±45 94±58 16.6%	09:40	234	20	36	973	8:91:1
Fire 3	Numbi	374±199 309±238 11.5%	13:20	150 (estimate)	31	26	941	2:96:2
Fire 4	Shabeni	147±120 115±127 19.5%	09:59	200	27	45	1095	–

* Abbreviation of "Nwaswitshaka".

ACPD
11, 3529–3578, 2011

Table 2. Spectral windows used for the forward model-based retrieval of biomass burning plume trace gas column amounts from the measured single beam spectra, selected from those used in previous closed-path biomass burning studies (e.g., Yokelson et al., 1997; Goode et al., 2000). Potentially interfering species (most importantly water vapour) were also included in the forward model parameterisation.

Trace gas species	Retrieval spectral window
Carbon dioxide (CO_2) and carbon monoxide (CO)	2020–2100 cm^{-1}
Methane (CH_4)	3010–3100 cm^{-1}
Formaldehyde (H_2CO)	2720–2840 cm^{-1}
Ammonia (NH_3)	900–940 cm^{-1}

ACPD
11, 3529–3578, 2011

Table 3. Molar emission ratios (Mol Mol^{-1}) and associated uncertainties for compound x with respect to CO ($ER_{x/CO}$) and CO_2 (ER_{x/CO_2}) for the backfire, headfire and residual smouldering combustion (RSC) stages of Fires 1 to 4, calculated using methods described in Sect. 3.5.1. Poorly constrained ERs (those with r^2 lower than 0.4) are not reported here. "Fire averaged" ERs are calculated using stage – specific ERs weighted by the FRE – determined proportion of fuel burned in each stage (apart from for Fire 4 where FRE data are unavailable). Uncertain ERs for the RSC stage do not prevent calculation of fire averaged values, since an insignificant amount of fuel is burned in this fire stage (Table 1). Final two rows show the mean $ER_{x/y} \pm 1\sigma$ calculated from the available fire averages, along with results for the same study area derived via aircraft sampling of plumes by Sinha et al. (2003a).

Fire	Fire stage	CO	CH_4		CH_2O		NH_3	
		ER_{x/CO_2} (×100)	ER_{x/CO_2} (×1000)	$ER_{x/CO}$ (×100)	ER_{x/CO_2} (×1000)	$ER_{x/CO}$ (×100)	ER_{x/CO_2} (×1000)	$ER_{x/CO}$ (×100)
1	Head	10.1±0.6	4.6±0.5	4.9±0.2	2.2±0.1	2.2±0.1	2.1±0.3	2.3±0.1
1	Back	11.4±0.5	6.0±0.4	5.2±0.4	3.2±0.4	2.8±0.3	1.8±0.2	1.5±0.2
1	RSC	9.5±1.3	6.7±1.2	7.5±0.4	1.7±0.3	1.8±0.2	3.2±0.5	3.5±0.1
	Fire 1 averaged	**10.3±0.6**	**4.8±0.5**	**5.0±0.2**	**2.3±0.2**	**2.3±0.1**	**2.1±0.3**	**2.2±0.1**
2	Head	6.2±0.6	2.4±0.4	3.9±0.5	1.2±0.2	2.0±0.2	–	1.4±0.2
2	Back	5.9±0.5	1.9±0.2	3.2±0.3	1.5±0.1	2.6±0.1		0.8±0.1
2	RSC	–	3.3±0.5	–	–	–	–	2.7±0.6
	Fire 2 averaged	**6.1±0.6**	**2.4±0.4**	**3.8±0.5**	**1.2±0.2**	**2.0±0.2**	**–**	**1.4±0.2**
3	Head	12.3±3.2	5.4±1.8	4.8±0.4	2.7±0.7	2.2±0.1	2.4±.1.0	2.3±0.3
3	Back	7.4±0.7	2.2±0.4	3.1±0.3	1.5±0.2	2.0±0.1	0.8±0.2	1.2±0.2
3	RSC	18.2±0.2	14.1±0.2	7.7±0.4	3.1±0.4	1.7±0.1	5.5±0.9	3.1±0.2
	Fire 3 averaged	**12.4±0.3**	**5.6±1.7**	**4.8±0.4**	**2.7±0.7**	**2.2±0.1**	**2.5±1.0**	**2.3±0.3**
4	Head	7.9±1.6	–	4.7±0.7	1.9±0.3	2.3±0.1	–	1.9±0.2
4	Back	6.9±0.4	2.1±0.2	3.2±0.2	1.8±0.1	2.6±0.8	0.9±0.1	1.5±0.1
4	RSC	22.4±1.4	13.1±1.1	6.0±0.2	4.2±0.3	1.9±0.1	6.5±0.5	3.0±0.1
	Mean and range of all fire averages (except Fire 4)	**9.6±3.2**	**4.3±1.7**	**4.5±0.6**	**2.1±0.8**	**2.0±0.3**	**2.3±0.3**	**2.0±0.5**
Sinha et al. (2003a)	Aircraft sampling	7.2±0.9	–	3.9±0.3	–	1.5±0.4	–	0.7±0.5

ACPD
11, 3529–3578, 2011

Table 4. Emissions factors ($g\,kg^{-1}$ of dry fuel burned) determined for the backfire, headfire and residual smouldering combustion (RSC) stages of Fires 1 to 4 calculated using methods described in Sect. 3.5.2. EFs based on poorly constrained ERs (see Table 3 and Fig. 7) are not shown here. "Fire averaged" EFs are calculated using the stage-specific EFs weighted by the FRE-determined proportion of fuel burned in each stage (apart from for Fire 4 where FRE data are unavailable). Weighted mean EF and associated uncertainty calculated according to Taylor (1997) is also shown. Comparison EFs for the same study area derived using different sampling and measurement techniques are listed, as are those for savannah and grassland fires reported in the widely used database of Andreae and Merlet (2001) and its more recent updates.

Fire no.	Emission factor	CO_2 ($g\,kg^{-1}$)	CO ($g\,kg^{-1}$)	CH_4 ($g\,kg^{-1}$)	CH_2O ($g\,kg^{-1}$)	NH_3 ($g\,kg^{-1}$)
1	Head	1655±166	106±12	2.8±0.4	2.5±0.3	1.3±0.2
1	Back	1632±163	118±13	3.6±0.4	3.6±0.6	1.1±0.2
1	RSC	1661±167	100±17	4.1±0.8	1.9±0.4	2.1±0.4
	Fire 1 averaged	**1652±165**	**108±13**	**2.9±0.4**	**2.6±0.3**	**1.3±0.2**
2	Head	1720±174	68±9	1.5±0.3	1.4±0.3	–
2	Back	1726±173	65±9	1.2±0.2	1.8±0.2	0.27±0.07
2	RSC	1827±183	–	2.2±0.4	–	–
	Fire 2 averaged	**1722±172**	**67±9**	**1.5±0.3**	**1.4±0.3**	**–**
3	Head	1701±177	127±36	3.2±1.1	3.0±0.8	1.5±0.65
3	Back	1701±170	80±11	1.4±0.3	1.7±0.3	0.53±0.14
3	RSC	1529±153	177±18	7.8±0.8	3.2±0.5	3.3±0.62
	Fire 3 averaged	**1697±176**	**127±35**	**3.3±1.1**	**1.5±0.8**	**1.5±0.64**
4	Head	1696±171	85±19	–	2.2±0.4	–
4	Back	1708±171	75±9	1.3±0.2	2.1±0.2	0.59±0.09
4	RSC	1477±149	211±25	7.0±0.2	4.2±0.5	3.71±0.47
	Fire averaged mean	**1689±99**	**100±7**	**2.1±0.2**	**2.0±0.2**	**1.3±0.2**
	Sinha et al. (2003a)	1700±60	68±30	1.7±1.0	1.1±0.38	0.26±0.14
	Cofer et al. (1996)	1610±380	55±13	3±2	–	–
	Andreae and Merlet (2001)	1613±95	65±20	2.3±0.9	0.26 to 0.44	0.6 to 1.05
	Andreae and Merlet (2009; personal communication)	1646±99	61±16	2.2±0.8	0.71±0.42	0.74±0.55
	Keene et al. (2006)	1319 to 1967	42 to 108	–	–	0.03 to 1.37
	Ward et al. (2006)	1643 to 1735	58 to 105	1.5 to 4.7	–	–

ACPD
11, 3529–3578, 2011

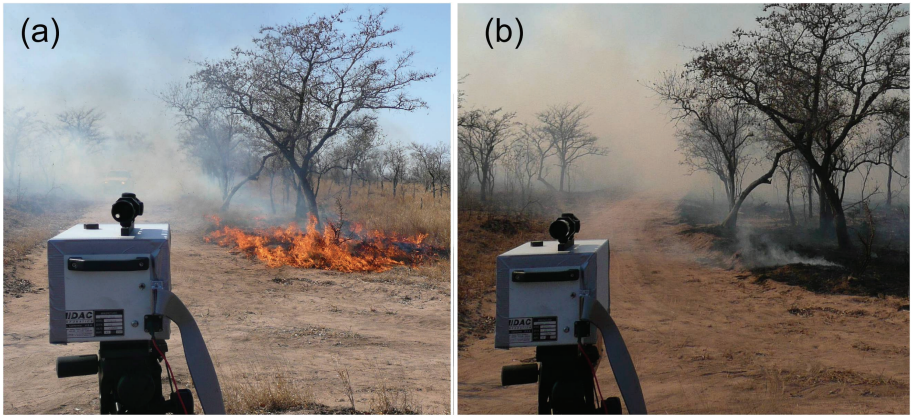

Fig. 1. Photography of the OP-FTIR deployment in Kruger National Park, taken from the same location and looking from the FTIR spectrometer towards the IR source. **(a)** Shows the situation shortly after backfire ignition, and **(b)** towards the end of the residual smouldering combustion (RSC) stage. Matching the geometry shown in Fig. 2, the spectrometer is located at the south-west corner of the plot to view the IR source located 150 m or more away along the N-S plot edge. Smoke is driven by the predominately westerly wind directly through the long optical path between the spectrometer and IR source. The source cannot be seen visually in these optical wavelength images due to scattering and obscuration by sub-micron sized smoke particulates, though this did not significantly impact the total energy signal recorded by the IR spectrometer (which measures at wavelengths >2.5 µm). Note the almost complete replacement of the grass fuel by char and ash in **(b)**, but the apparently very limited fire impact on the larger trees.

ACPD
11, 3529–3578, 2011

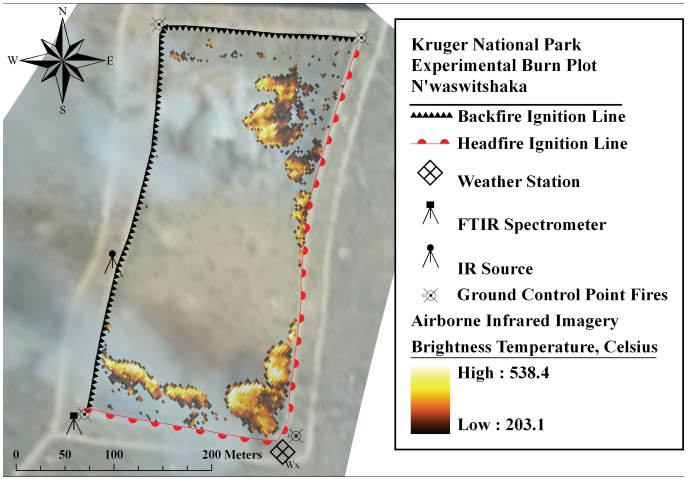

Fig. 2. Typical field setup deployed here to study the smoke characteristics of Southern African savannah fires using OP-FTIR spectroscopy. Data are from a period less than halfway through the fires duration, when the flaming front had only transited across approximately one quarter of the total plot area. Background view is a frame captured from the near vertically-viewing optical video record made from the hovering helicopter. Superimposed on this is the map of pixel brightness temperatures recorded via an airborne AGEMA-550 infrared camera. Only the locations of ground pixels whose IR brightness temperature (BT) exceeds 203 °C (476 K) are displayed, corresponding to areas of active combustion. Higher BTs are generally seen at the fire fronts (likely flaming areas), whereas lower BTs are recorded behind the fonts, i.e., in the "smoking zone" identified by Lacaux et al. (1996) and where combustion rate is interpreted to be lower. It should be noted that BTs are unlikely to represent actual fire temperatures since the flames may under-fill pixels (see e.g., Wooster et al., 2005). Smoke plumes (grey) can be seen emanating from areas of active combustion. The backfire (downwind) and headfire (upwind) ignition lines are indicated, as is the location of the FTIR spectrometer, IR source and weather station. Data are from Fire 1 (Table 1) and all imagery and spatial locations were positioned using GPS records and/or ground control points identified in either the optical or IR video records.

ACPD
11, 3529–3578, 2011

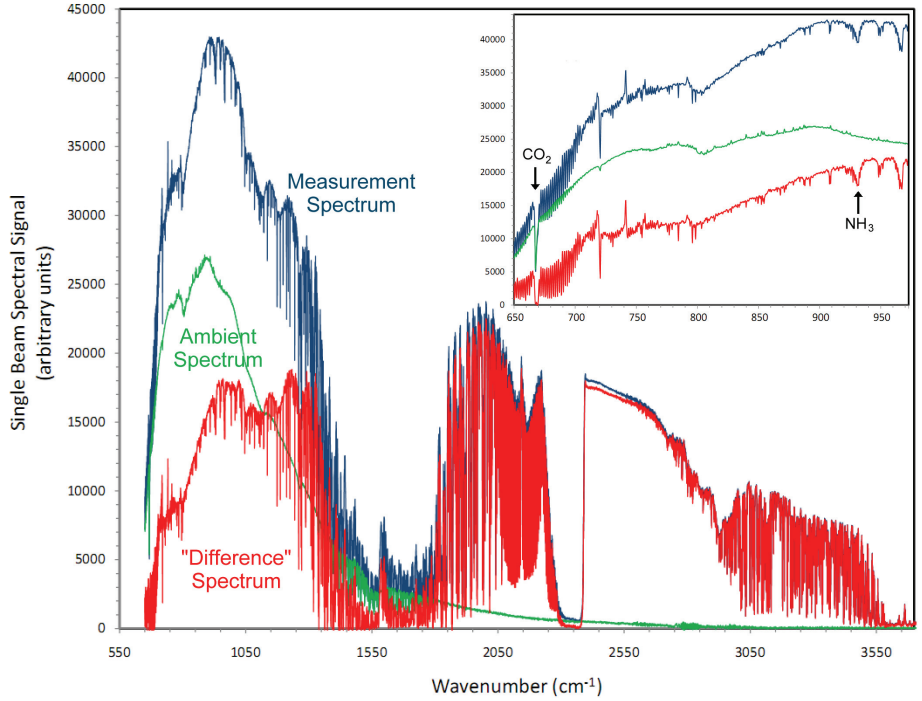

Fig. 3. Single beam measurement spectrum (blue) collected by the FTIR spectrometer viewing the IR Source across a 170 m smoke-filled optical path during Fire 1. Also shown is an "ambient" spectrum (green) collected without the IR source, together with the resulting "difference" spectrum (red) calculated according to Müller et al. (1999) to remove the effect of ambient emission (including instrument self-emission) from the measurement spectrum prior to trace gas retrieval. The inset focuses on the spectral range where the ambient spectrum has most significance (i.e., lower wavenumbers). The 668–670 cm^{-1} CO_2 absorption band is correctly seen to show zero signal in the "difference" spectrum, whilst the primary 925–934 cm^{-1} absorption feature used here to retrieve NH_3 column amounts is clearly apparent in both the measurement and difference spectra.

ACPD
11, 3529–3578, 2011

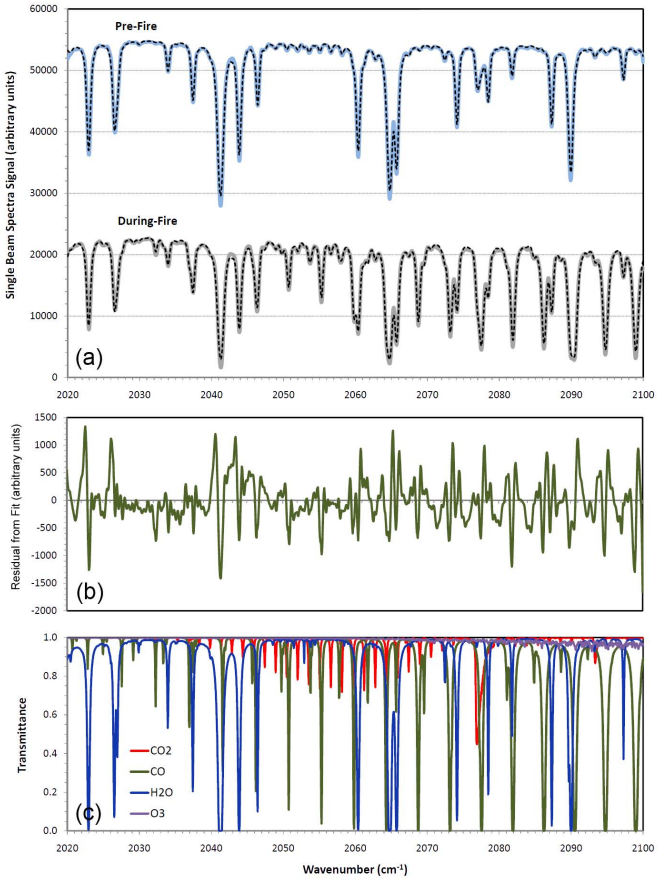

Fig. 4. Caption on next page.

ACPD
11, 3529–3578, 2011

Fig. 4. Open path FTIR single beam spectra and best-fit forward modelled spectra for two example measurements recorded during Fire 1 (Table 1). Spectra were recorded by the deployed FTIR spectrometer operating in extended open path mode at 0.5 cm^{-1} wavenumber resolution, and the spectral window shown is the 2020–2100 cm^{-1} range used here for retrieval of CO_2 and CO abundances (Table 2). **(a)** Examples of single beam spectra measured both prior to and subsequent to fire ignition, with the best-fit forward modelled spectra calculated using the retrieval procedure of Burton (1998) overlain in each case (dashed lines). The pre-fire and during-fire spectra correspond, respectively, to times 5 and 22 min into the trace gas time series shown in Fig. 5. Pre- and during-fire spectra are shown offset for clarity. Note the greater number of strong absorption features in the during-fire spectra, caused by the increased within-plume trace gas abundances. **(b)** The residual of the measured and best-fit forward modelled "during fire" spectra shown in **(a)**, indicating that no significant spectral features remain unfitted and confirming the strong agreement between the measured and forward-modelled spectra seen in **(a)**. Retrievals of CO_2/CO column amounts from the pre-fire and during-fire spectra are equivalent to the ratio of path averaged mixing ratios (in ppmv) of 416/0.12 (pre-fire) and 824/49 (during-fire), respectively. **(c)** The transmittance spectrum of the best-fit CO_2, CO and H_2O column amounts calculated from the during-fire spectra shown in **(a)**. The product of these transmittances and the background polynomial provides the best-fit modelled spectra already shown in **(a)**. Other gases (e.g., N_2O, OCS) having absorption features within this spectral window were included in the fit, but none were found in significant quantities.

ACPD
11, 3529–3578, 2011

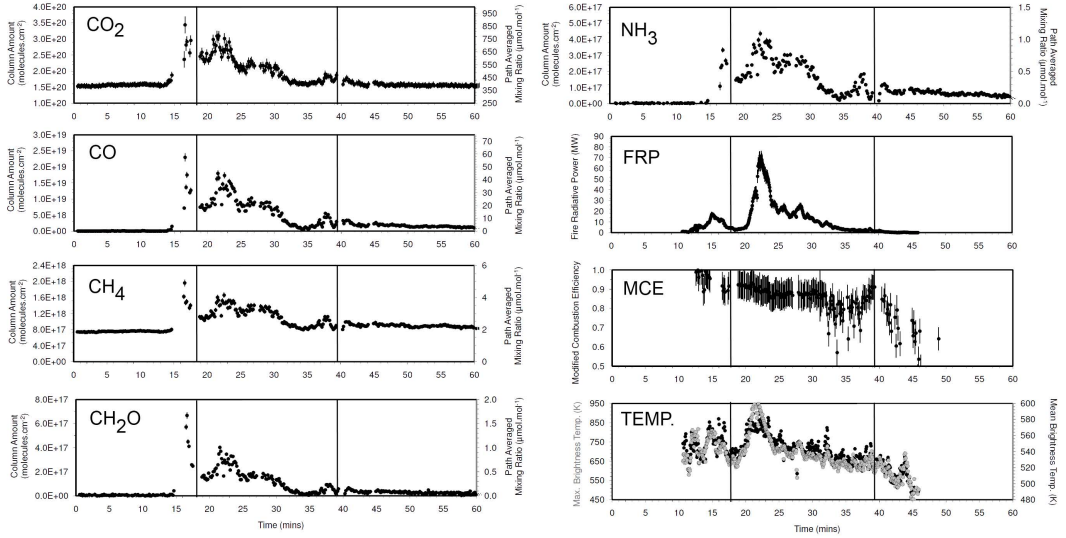

Fig. 5. Time-series of trace gas column amounts, Fire Radiative Power, Modified Combustion Efficiency (MCE) and fire temperature for Fire 1 (Figs. 2–4 and Table 2). Trace gas abundances are expressed as path-integrated column amounts (molecules cm^{-2}), with the equivalent path averaged mixing ratio shown on the r.h.s. y-axis. After the 14:01 LT ignition time (time>10 min on this plot) these mixing ratios represent a weighted average of the pure plume and ambient air abundances (see Sect. 3). Error bars for the trace gas retrievals are calculated from the residuals of the best-fit forward modeled spectra (Horrocks et al., 2001), whilst those for FRP are calculated according to Wooster et al. (2005).

ACPD
11, 3529–3578, 2011

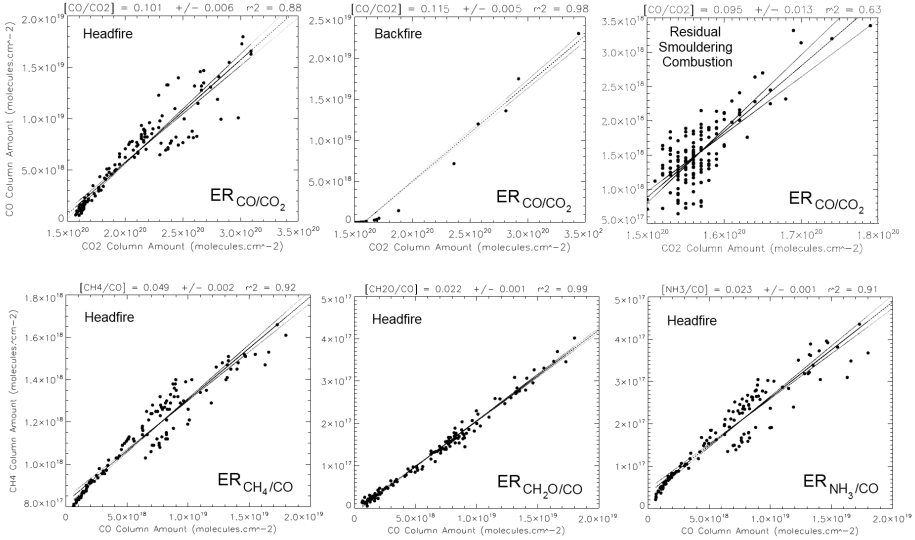

Fig. 6. Example 2-D scatterplots of the measured trace gas column amounts used to calculate emissions ratios. Data are from Fire 1, whose time-series measurements are shown in Fig. 5. Top row shows the CO vs. CO_2 data for the backfire, headfire and residual smouldering combustion stages of this fire. Bottom row shows the CH_4 vs. CO; CH_2O vs. CO and NH_3 vs. CO data for the headfire stage only. The slope of the least squares linear best fit to these data (shown, along with its uncertainty) is used to derive the relevant emission ratio ($ER_{x/y}$), whose value is shown above the relevant plot. Note the different axes scales required to accommodate the varying column amounts measured during the various fires stages.

ACPD
11, 3529–3578, 2011

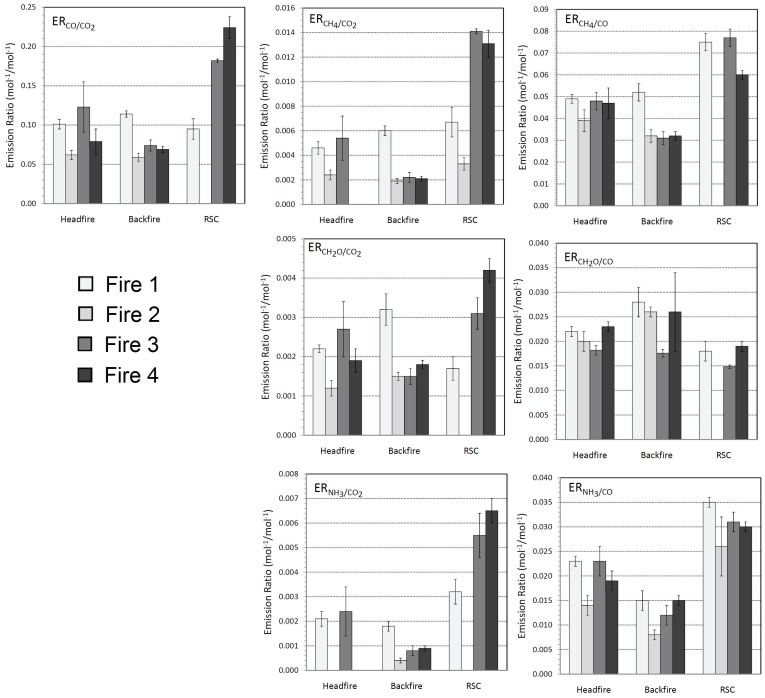

Fig. 7. Emission ratios for CO_2, CO, CH_2O and NH_3 for the backfire, headfire and residual smouldering combustion (RSC) stages of Fires 1–4 (see Table 1 for fire details). ERs to both CO and CO_2 are shown, and missing values indicate cases where the derived $ER_{x/y}$ was poorly constrained based on a low coefficient of determination (r^2) between the two relevant trace gas column amounts. This maybe due in some cases to short periods where the plume blew outside of the optical path, and in others to instances where the relationship between the two trace gas column amounts is not well described by a linear fit. ER uncertainties are given by the error bars, derived from the 95% confidence limits in the slope of the least squares linear best fit to the trace gas column amounts (see Fig. 6).

ACPD
11, 3529–3578, 2011

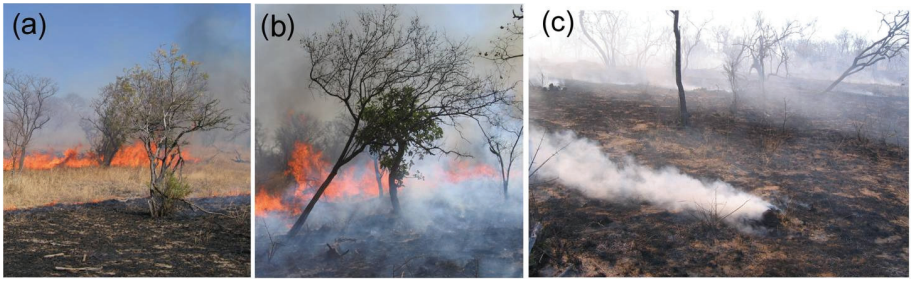

Fig. 8. Photographs of the experimental fires taken during **(a)** the headfire of Fire 2 (Skukuza) and **(b)** the headfire of Fire 1 (N'waswitshaka), with the flaming fronts moving away from the photographer in each case. Note the substantial "smoking zone" in **(b)** in comparison to **(a)**. Photograph **(c)** is also of the N'waswitshaka plot (Fire 1), and demonstrates the effect that elephant dung located in the plot interior had on the amount of smouldering combustion. This is expected to have contributed significantly to emissions from the headfire "smoking zone" seen in **(b)**.

ACPD
11, 3529–3578, 2011

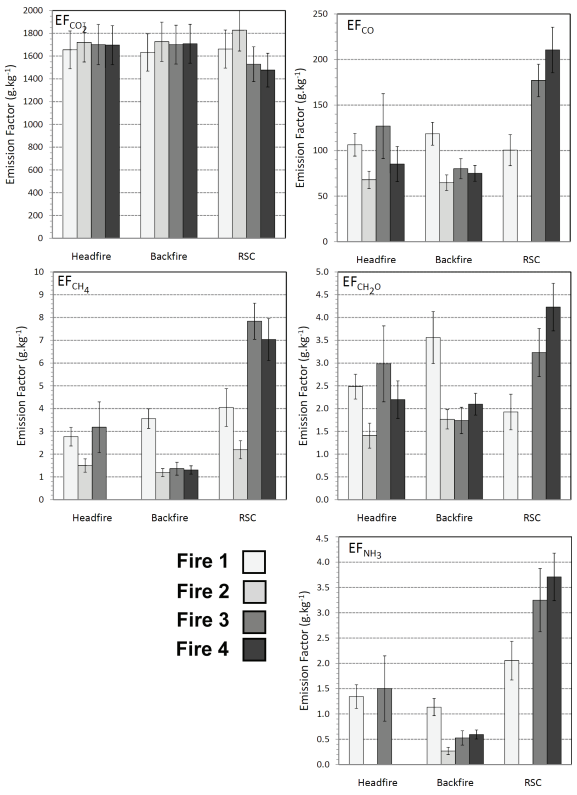

Fig. 9. Emissions factors [EF_x] for CO_2, CO, CH_2O and NH_3 for the backfire, headfire and residual smouldering combustion stages (RSC) of Fires 1–4 (see Table 1 for fire details). Error bars provide a measure of emissions factor uncertainty, derived in quadrature from the uncertainty in the relevant emission ratios and a ±10% uncertainty in the assumed fuel C content. Missing values represent cases where the relevant ER_{x/CO_2} measure was poorly constrained based on a low coefficient of determination (r^2) between the two relevant trace gas column amounts (see Fig. 7).

ACPD
11, 3529–3578, 2011